



## King's Research Portal

DOI:

[10.1016/j.molliq.2020.114892](https://doi.org/10.1016/j.molliq.2020.114892)

*Document Version*

Peer reviewed version

[Link to publication record in King's Research Portal](#)

*Citation for published version (APA):*

Valero, M., Hu, W., Houston, J. E., & Dreiss, C. A. (2021). Solubilisation of salicylate in F127 micelles: Effect of pH and temperature on morphology and interactions with cyclodextrin. *JOURNAL OF MOLECULAR LIQUIDS*, 322, Article 114892. <https://doi.org/10.1016/j.molliq.2020.114892>

### **Citing this paper**

Please note that where the full-text provided on King's Research Portal is the Author Accepted Manuscript or Post-Print version this may differ from the final Published version. If citing, it is advised that you check and use the publisher's definitive version for pagination, volume/issue, and date of publication details. And where the final published version is provided on the Research Portal, if citing you are again advised to check the publisher's website for any subsequent corrections.

### **General rights**

Copyright and moral rights for the publications made accessible in the Research Portal are retained by the authors and/or other copyright owners and it is a condition of accessing publications that users recognize and abide by the legal requirements associated with these rights.

- Users may download and print one copy of any publication from the Research Portal for the purpose of private study or research.
- You may not further distribute the material or use it for any profit-making activity or commercial gain
- You may freely distribute the URL identifying the publication in the Research Portal

### **Take down policy**

If you believe that this document breaches copyright please contact [librarypure@kcl.ac.uk](mailto:librarypure@kcl.ac.uk) providing details, and we will remove access to the work immediately and investigate your claim.

1  
2 Solubilisation of salicylate in F127 micelles: effect of pH and temperature  
3 on morphology and interactions with cyclodextrin  
4

5 Margarita Valero,<sup>\*a</sup> Wenjing Hu<sup>b</sup>, Judith E. Houston<sup>c,d</sup>, Cécile A. Dreiss<sup>b</sup>

6  
7 <sup>a</sup> Dpto. Química Física, Facultad de Farmacia, Universidad de Salamanca, Campus  
8 Miguel de Unamuno, s/n, 37007 Salamanca, Spain

9 <sup>b</sup> Institute of Pharmaceutical Science, King's College London, Franklin-Wilkins  
10 Building, 150 Stamford Street, London SE1 9NH, U.K.

11 <sup>c</sup> Jülich Centre for Neutron Science (JCNS) at Heinz Maier-Leibnitz Zentrum (MLZ)  
12 Forschungszentrum Jülich GmbH, Lichtenbergstraße 1, 85747 Garching, Germany.

13 <sup>d</sup> European Spallation Source (ESS), Odarslövsvägen 113, 225 92 Lund, Sweden.  
14

15 \*Corresponding author: mvalero@usal.es

16  
17 **Abstract**

18 The present work examines the behavior of salicylic acid (SAL)-loaded F127 micelles as  
19 drug nanocarriers for controlled release by means of interaction with 2,6-dimethyl- $\beta$ -  
20 cyclodextrin (DIMEB) in the intestine at basic pH=7-8, both important excipients, of  
21 pharmaceutical formulations.

22 The results show that acidic pH (pH=1) strongly increases the partitioning of SAL in F127  
23 micelles compared to neutral pH, due to the drug being in its molecular form.  
24 Fluorescence spectroscopy and small-angle neutron scattering show that free and SAL-  
25 loaded F127 micelles transition to cylindrical micelles at pH=1 and high temperatures  
26 (37°C). Micelles loaded with SAL are disrupted by DIMEB to a higher extent than at pH=7  
27 at physiological temperature. This study reveals that F127 could be a valuable nanocarrier  
28 for intestine controlled release of SAL. Taken together, our results highlight the  
29 importance of water in the structure of the micelles and their interaction with DIMEB, and  
30 bring precious insights into the mechanisms that regulate drug loading and release in  
31 complex formulations.

32  
33 **Key words**

ABBREVIATIONS

SAL: Salicylic acid

PPO: polypropylene oxide

PEO: polyethylene oxide

NR: Nile red

DIMEB: heptakis (2,6-di-O-methyl)- $\beta$ -cyclodextrin

SANS: Small angle neutron scattering

CP: Cloud Point

34 Salicylic acid (SAL); Pluronic® F127; 2,6- dimethyl  $\beta$ -cyclodextrin (DIMEB);  
35 cylindrical micelles; controlled release; small angle neutron scattering (SANS),  
36 fluorescence spectroscopy.

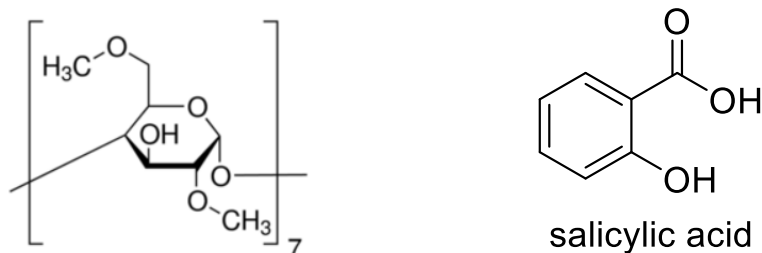
37

## 38 **1. Introduction**

39 Pluronics are a family of tri-block co-polymers formed by two lateral hydrophilic  
40 polyethylene oxide chains (PEO), and a central hydrophobic polypropylene oxide block  
41 (PPO),  $(\text{PEO})_x\text{-(PPO)}_y\text{-(PEO)}_x$ . Pluronic F127, also known as poloxamer 407, is a  
42 member of the family with composition  $(\text{PEO})_{100}\text{-(PPO)}_{65}\text{-(PEO)}_{100}$ . As other Pluronics,  
43 F127 forms core-shell micelles (CS-micelles) above its critical micelle concentration  
44 (cmc), with a hydrophobic central core formed of PPO chains surrounded by a hydrophilic  
45 shell, which comprises the PEO blocks. Pluronic F127 has been widely studied as a drug  
46 carrier and is approved by the FDA and the British Pharmacopeia as an excipient for drug  
47 delivery after oral administration. F127 has demonstrated attractive properties in the  
48 pharmaceutical field such as improvement of the oral bioavailability of drugs [1–5] and  
49 the ability to incorporate into membranes [6,7], increasing the efficiency of anti-cancer  
50 resistant drugs [1,8] owing to its ability to inhibit glycoprotein G [9,10]. In addition,  
51 Pluronic F127 can also be envisaged for topical formulations, since it forms gels close to  
52 body temperature [11–15].

53 Recently, we have investigated the ability of F127 to load drugs with varying chemical  
54 structures [16–18] and how their release can be modulated by the interaction with  
55 cyclodextrins, another well-known pharmaceutical excipient.

56 Cyclodextrins are cyclic oligosaccharides made of glucose units that present a truncated  
57 conical shape. They have an inner apolar domain formed by the ether groups. Their  
58 hydrophilic external edges are lined with primary and secondary alcohol groups  
59 protruding out of the inner cavity, which can be further modified to improve their  
60 solubility or functionality. This unusual cyclic structure with an apolar interior gives  
61 cyclodextrins the ability to form inclusion complexes with different chemical compounds,  
62 in particular drugs, or thread polymer chains in structures referred to as  
63 pseudopolyrotaxanes (PPRs) [19,20]. The methylated derivative of  $\beta$ -cyclodextrin ( $\beta$ -CD,  
64 a 7-glucose unit construct), namely, heptakis (2,6-di-O-methyl)- $\beta$ -cyclodextrin (DIMEB)  
65 (Scheme 1), has been shown to modulate the micellization of a range of PEO-based  
66 micellar aggregates [21–23], including free and drug-loaded F127 micelles [16–18],  
67 inducing – in certain conditions – full rupture of the micelles and therefore releasing a  
68 payload. It is clear from our previous work that temperature, the specific chemical  
69 structure of the drug and its precise localization within the micelle can all modulate the  
70 interaction between the micelle and DIMEB, and hence the extent of micellar disruption  
71 [16–18].



**Scheme 1:** Chemical structure of the basic unit of DIMEB (*left*) and salicylic acid (*right*).

However the rules that govern this modulation are still not understood; for instance, while the formation of PPRs as the lever that induces micellar rupture has been excluded, and possible external interactions between PO units and cyclodextrins envisaged instead [24], it is not clear how the presence of drugs in the micellar compartments modulate this interaction [17,18]. While it has now been shown that cyclodextrins can induce full demicellization, the control of the process under desired conditions is elusive. Therefore, an understanding of the mechanisms that underlie this process is needed to harness the potential of DIMEB in pharmaceutical formulations. Most of the studies carried out with F127, drugs and DIMEB were conducted at pH=7, but very few have been reported at acidic pH [16]. Following oral administration, drugs go through a range of pH in the gastrointestinal tract, ranging from 1 to 9, however very few studies have explored the behaviour of free F127 micelles at this pH [25], or other Pluronic [26–28]. The solubility of ionizable drugs varies considerably at this pH and compromise drug bioavailability [29]. Therefore, it is of interest to study the effect of acidic pH on these and other properties of F127, both free and loaded with acid-basic compounds.

Salicylic acid (SAL) (Scheme 1) is considered the most ancient remedy currently in use [30]. Recently, it has received great attention in the food and agriculture fields, since SAL is a hormone produced by some plants involved in the resistance against microbial pathogens and anti-cancer response [31]. It would therefore be potentially useful in human therapy against these pathologies, but the gastrointestinal side effects make its oral administration impossible. On the other hand, SAL is the only non-steroidal anti-inflammatory drug (NSAID) with a potent keratolytic activity [32] and therefore it is widely used in topical applications, both in cosmetics and dermatological consumer products. High drug concentrations are allowed in these formulations, up to 2% (w/w) for acne treatment by the Food and Drug administration, (FDA) [33], or up to 3% in leave-on and rinse-off, and in cosmetics such as face and general creams, shower gels, shampoos, etc by the Europe Cosmetics Regulation EC 1223/2009. Salicylic acid is absorbed through the skin from topical formulations; the percutaneous absorption is strongly dependent on the pH [34], but in most of the formulations cited above, the pH is not controlled. In this context, the development of new SAL formulations intended for oral and topical administrations is a worthy endeavour. For this purpose, we need a fundamental understanding of the effect of pH on loading capacity and solubilization locus and on how micellar morphology and properties are affected by the presence of the drug, and, in turn, by interactions with cyclodextrin used as a handle for drug release; this knowledge will help tailor formulations to desired outcomes.

111 Based on these considerations, the present work gives a detailed characterization of F127  
112 micelles, free and loaded with the drug salicylic acid at pH=1, over a range of  
113 temperatures, in the absence and presence of DIMEB, which acts as a micellization-  
114 modulator. We use small-angle neutron scattering (SANS) to examine the morphology of  
115 the free and drug-loaded micelles under a range of conditions, in the absence and presence  
116 of DIMEB. Fluorescence and UV-Vis spectroscopies are employed to measure the  
117 partitioning of the drug withing the micelles, its binding to cyclodextrins, and shed light  
118 on the localization of SAL in the micelles, to bring an understanding into these complex  
119 three-way interactions (drug-micelles-cyclodextrin), which determine the state of  
120 aggregation of the drug nanocarrier and hence drug loading and release. Our results form  
121 the basis for a formulation rationale and highlight the importance of water in the  
122 interactions.

123

## 124 **2. Experimental Section**

### 125 2.1. Materials

126 Pluronic copolymer F127 comprising a central block of 65 PPO units and two side-blocks  
127 of PEO (100 units each) was obtained from Sigma-Aldrich UK ( $M_w = 12,600$ ). Heptakis  
128 (2,6-di-*O*-methyl)- $\beta$ -cyclodextrin (DIMEB) was obtained from Sigma-Aldrich UK  
129 (H0513,  $M_w = 1331.4 \text{ g mol}^{-1}$ ).

130 The drugs sodium salicylate (SAL, 71945) and salicylic acid (SAL, 84210), Nile red (NR,  
131  $M_w 318.4 \text{ g}\cdot\text{mol}^{-1}$ ), HCl (320331) ACS reagent, 37%, as well as D<sub>2</sub>O (151882) with a  
132 purity of 99.9 %, were purchased from Sigma Aldrich. The aqueous solutions were  
133 prepared using Milli-Q water or D<sub>2</sub>O as specified.

134 All materials were used as received.

135

### 136 2.1. Sample Preparation

137 Aqueous and D<sub>2</sub>O stock solutions of sodium salicylate (1) alone, (2) with F127, and (3)  
138 with DIMEB, as well as (4) F127 alone, were prepared by weight. Aqueous and D<sub>2</sub>O stock  
139 solutions of 0.2M HCl and DCl, respectively, were prepared. For partition coefficient  
140 determination by fluorescence, solutions of constant drug and different F127  
141 concentrations were prepared by mixing the appropriate amount of solutions (1) and (2).  
142 Two regimes of drug concentration were studied: dilute ( $1.5 \cdot 10^{-3} \text{ wt}\%$ ) and concentrated,  
143 0.16 wt%, limited by the aqueous solubility ( $S_0 < 0.2\% \text{ (w/v)}$ ) found for sodium salicylate  
144 at pH=1 and 25°C.

145 For the determination of the CD-drug binding constant, solutions at constant drug and  
146 different CD concentrations were prepared by mixing solutions (3) and (1). In both cases,  
147 the required amount of DCl or HCl to achieve pH=1 was added.

148 For the determination of partition by uv-vis spectroscopy, a fixed amount of salicylic acid  
149 was weighed and a constant amount of F127 solution at different concentrations, prepared  
150 from solution (4), was added. After adding the amount of DCl or HCl needed to obtained  
151 the desired pH, the solutions were kept stirring over a week at room temperature. The pH  
152 of saturated solutions was corrected to achieve the same final pH in all the samples. The

153 excess of solid drug was removed by centrifugation. Samples were diluted and the pH  
154 corrected again before uv-vis absorption measurement.

155 For the determination of the critical micellar concentration (cmc), solution (2) was diluted  
156 to produce a range of F127 concentrations. The cmc value of F127 at pH=1 used to  
157 determine partition was obtained by dynamic light scattering (DLS) as cmc= 0.04 wt %.

158 A F127 molar volume of  $\bar{V}=10.8$  L/mol, was experimentally obtained by density  
159 measurements with a pycnometer, at room temperature.

160 Samples for cloud point measurement were prepared by weighting the appropriate amount  
161 of salicylic acid (and sodium chloride, when added), and further addition of the required  
162 amount of F127 (2) and DCI stock solutions, completing with D<sub>2</sub>O. All solutions were  
163 prepared by weight and then most of the concentration units refer to weight %.

164 Appropriate volumes of concentrated NR stock solution in ethanol ( $4.66 \cdot 10^{-3}$  M) were  
165 taken, to achieve a final NR concentration of  $4.66 \cdot 10^{-6}$ M, then the solvent was evaporated.  
166 The residue was then solubilized in either water, 5 wt% F127, or 5 wt% F127 1wt% SAL  
167 aqueous solutions at pH=1.

168

### 169 2.3. Methods

#### 170 *2.3.1. UV-vis absorption spectroscopy*

171 The absorption spectra of SAL and NR were obtained in a Perkin Elmer UV/Vis  
172 spectrometer (Lambda 2).

173 The UV absorption of the drug was measured at  $\lambda=300$  nm, corresponding to the isosbestic  
174 point for molecular and ionized SAL, using a Perkin Elmer UV/Vis spectrometer (Lambda  
175 2). Solubility was determined using the molar absorptivity value,  $\epsilon_{300}^{\text{H}_2\text{O}}= 3550 \text{ M}^{-1} \text{ cm}^{-1}$   
176 experimentally obtained. The increase in SAL solubility with F127 addition was  
177 quantified as the ratio  $S_{0,\text{F127}}/S_{0,\text{H}_2\text{O}}$ , where  $S_{0,\text{F127}}$  is the solubility of SAL at a given F127  
178 concentration and  $S_{0,\text{H}_2\text{O}}$  the solubility of SAL in water.

179 All the experiments were carried out at 25°C.

180

#### 181 *2.3.2. Steady- State Fluorescence spectroscopy*

182 Measurements were performed on a Cary Eclipse fluorescence spectrophotometer  
183 (Varian, Oxford, UK).

184 The excitation wavelength used for salicylic acid was  $\lambda_{\text{exc}}= 296$  nm. Emission intensity  
185 variation was followed at  $\lambda_{\text{em}}= 440$  nm.

186 The binding constant of the drug to F127 micelles,  $K_{\text{F127}}$ , was determined at two drug  
187 concentrations:  $1.5 \cdot 10^{-3}$  wt% and 0.16 wt%, using the method proposed by Almgren [35]  
188 and the mathematically modified equation (Eq.1), as described elsewhere [18].

189

$$190 \left( \frac{F_0}{F-F_0} \right) = \left( \frac{F_0}{F_\infty-F_0} \right) \left( 1 + \frac{1}{K_{\text{F127}}C_M} \right) \quad \text{Eq. (1)}$$

191

192

193

194 where  $C_M$  is the micellized surfactant concentration with  $C_M = (C_S - \text{cmc})$ ,  $C_S$  being the  
 195 total surfactant concentration,  $F$  is the measured fluorescence intensity,  $F_0$  and  $F_\infty$  are the  
 196 fluorescence intensity when all the drug is free and complexed, respectively.  $K_{F127}$  is the  
 197 binding constant of the drug to the micelle, obtained by fitting the experimental data. The  
 198 critical micelle formation of F127 at pH=1,  $\text{cmc} = 4 \cdot 10^{-2} \text{wt\%}$ , estimated from dynamic  
 199 light scattering (DLS) data, was used.

200  $F_0$  was obtained from experimental data, while  $F_\infty$  was obtained by fitting and further  
 201 comparing to the experimental value as a control of the fitting model. The  $F_\infty$  value  
 202 obtained from the fitting (y-intercept) reproduces reasonably well the experimental value  
 203 of this parameter.

204 Plots of  $F_0/(F-F_0)$  vs  $1/C_M$  give a linear plot, where the ratio of the y-intercept over the  
 205 slope gives  $K_{F127}$ .

206 The concentration of F127 was expressed in mass fraction (X) for consistency of units  
 207 between all experiments; as a result, the binding constant, which is expressed in inverse  
 208 of concentration units,  $X^{-1}$ , is given in g/g.

209 The partition coefficient, P, can be calculated from the binding constant,  $K_{F127}$ , using  
 210 Eq.(2) [36] as previously reported [17].

$$211 \quad 212 \quad K_{F127} = (P-1) \bar{V} \quad \text{Eq. (2)} \quad 213$$

214 where  $K_{F127}$  is the binding constant of SAL to F127,  $M^{-1}$  (conversion from  $X^{-1}$  was made  
 215 using  $\delta_{F127}=1.0099 \text{ g/mL}$ , obtained experimentally at  $25^\circ\text{C}$ );  $\bar{V}$  is the partial molar volume  
 216 of F127 ( $\bar{V}=10.8 \text{ L/mol}$ , experimental value).

217 The binding constant of the drug ( $[\text{SAL}] = 1.5 \cdot 10^{-3} \text{ wt\%}$ ) to the cyclodextrin,  $K_{DIMEB}$ , was  
 218 determined as described previously [17,18] by fitting fluorescence intensity at  $\lambda=440 \text{ nm}$ ,  
 219 to Eq (3).

$$220 \quad 221 \quad F = \frac{(F_0 + F_\infty K_{DIMEB} [CD])}{1 + K_{DIMEB} [CD]} \quad \text{Eq. (3)} \quad 222$$

223 where  $F$  is the measured fluorescence intensity,  $F_0$  and  $F_\infty$  are the fluorescence intensity  
 224 when all the drug is free and complexed, respectively; both of them are experimental  
 225 values.  $[CD]$  is the concentration of free cyclodextrin, which, in these dilute systems,  
 226 corresponds to the analytical concentration, since  $[CD] \gg [\text{drug}]$ . A non-linear least  
 227 squares method was used to fit the experimental results to Eq (4) and obtain  $K_{DIMEB}$ . The  
 228  $[CD]$  concentration used was expressed in mass fraction (X) for consistency of units  
 229 between all experiments; as a result, the binding constant, which is expressed in inverse  
 230 of concentration units,  $X^{-1}$ , is in g/g.

231 Both studies were carried out using  $\text{H}_2\text{O}$  as a solvent. For comparative purposes, some  
 232 experiments were also performed in  $\text{D}_2\text{O}$ .

233

### 234 2.3.3. Small-Angle Neutron Scattering (SANS)

235 SANS experiments were carried out on the KWS-2 diffractometer at the Jülich Centre for  
 236 Neutron Science (JCNS), München, Germany [37]. An incidental wavelength of  $5 \text{ \AA}$  was  
 237 used with detector distances of 1.7 and 7.6 m and a collimation length of 8 m, to cover a  
 238 momentum transfer,  $q$ , range from 0.008 to  $0.5 \text{ \AA}^{-1}$ . In the standard mode, a wavelength

239 spread  $\Delta\lambda/\lambda = 20\%$  was used. All samples were measured in quartz cells (Hellma) with a  
 240 path length of 2 mm using D<sub>2</sub>O as the solvent. The samples were placed in an aluminium  
 241 rack where water was recirculated from an external Julabo cryostat, at 20-50°C. This set-  
 242 up enables a thermal control with up to 0.1 °C precision. Scattered intensities were  
 243 corrected for detector pixel efficiency, empty cell scattering and background due to  
 244 electronic noise. The data were set to absolute scale using Plexiglas as a secondary  
 245 standard. The obtained macroscopic differential cross-section  $d\Sigma/d\Omega$  was further  
 246 corrected for contribution from the solvent. The complete data reduction process was  
 247 performed with the QtiKWS software provided by JCNS in Garching [37].

248 Solutions of F127 5 wt% with 1 wt% salicylate sodium salt at pH=1 were prepared.  
 249 DIMEB concentrations, when added, ranged from 5 to 11 wt%. All samples were  
 250 measured in D<sub>2</sub>O to optimize the contrast and minimize the incoherent background for  
 251 SANS experiments.

252 SANS curves, after subtraction of the background, were fitted using SAS View 4.2.1.  
 253 software [38] to a core-shell sphere model (CSS) [39] (curves at 20-37°C) or core-shell  
 254 cylinder (CSC), [40,41] (curves at 37 and 50 °C), which were combined to a hard-sphere  
 255 (HS) structure factor. Except in SAL-loaded F127 micelles at 50°C, a contribution of  
 256 random coils, with  $R_g = 7-12 \text{ \AA}$ , from PEO, was considered, as in previous work [18,42].  
 257 The size polydispersity of the micellar core, shell thickness and length (for the CSC) were  
 258 fixed for each set of data to minimize the number of fitting parameters to: 0.15/0.20 (C/S)  
 259 at 20-37°C (CSS) and 0.15/0.2/0.1 (C/S/L) at 37 and 50 °C (CSC). In the SAL-loaded  
 260 micelles, polydispersity was fixed to 0.15/0.15 at 20, 25 °C; 0.10/0.20 at 37 °C, (CSS);  
 261 and 0.10/0.20/0 at 37 and 50 °C (CSC).

262 The curves of SAL-loaded micelles in the presence of DIMEB were fitted to a core-shell  
 263 sphere (CSS) [39] with additional spheres of  $R = 9 \text{ \AA}$  to account for DIMEB (5% DIMEB)  
 264 or poly-gaussian coils  $R_g = 11$  and  $13 \text{ \AA}$  (at 7 and 9 wt% DIMEB, respectively). With 11  
 265 wt% DIMEB, a poly-gaussian coils model [43–45], with a sphere contribution ( $R = 32 \text{ \AA}$ )  
 266 was used. The scattering length density of DIMEB was fixed at  $\text{sld}_{\text{DIMEB}} = 1.89 \times 10^{-6} \text{ \AA}^{-2}$ .  
 267 The size polydispersity was fixed at 0.16 in all cases.

268 In order to reduce the number of fitting parameters, in all the fits, the sld of the core was  
 269 initially fixed at  $\text{sld}_{\text{PO}} = 0.4 \times 10^{-7} \text{ \AA}^{-2}$ , reflecting a very dehydrated core, as observed for  
 270 other poloxamines, [17,18,21,46,47]. This value was kept constant at temperatures 20-  
 271 37°C, but at 37 and 50 °C it was a floating parameter.

272 The water content of each part of the aggregate was determined from the corresponding  
 273 sld returned by the fits from Equation (4).

$$274 \quad \text{sld}_{\text{core/shell}} = X_{\text{PPO/PEO}} \times \text{sld}_{\text{PPO/PEO}} + X_{\text{D}_2\text{O}} \times \text{sld}_{\text{D}_2\text{O}} \quad \text{Eq. (4)}$$

275 with  $\text{sld}_{\text{PPO}} = 4 \times 10^{-7}$  or the value obtained from the fits (see above);  $\text{sld}_{\text{PEO}} = 6.70 \times 10^{-7}$ ;  $\text{sld}_{\text{D}_2\text{O}} = 6.36 \times 10^{-6}$ .

277

278 *2.3.5. Cloud Point (CP) determination*



279 Cloud points were determined by visual observation of the turbidity of the samples (in 1.5  
280 mL eppendorf) immersed in a water bath. The temperature was increased by 1°C intervals  
281 up to phase separation. All measurements were made in triplicates.

282

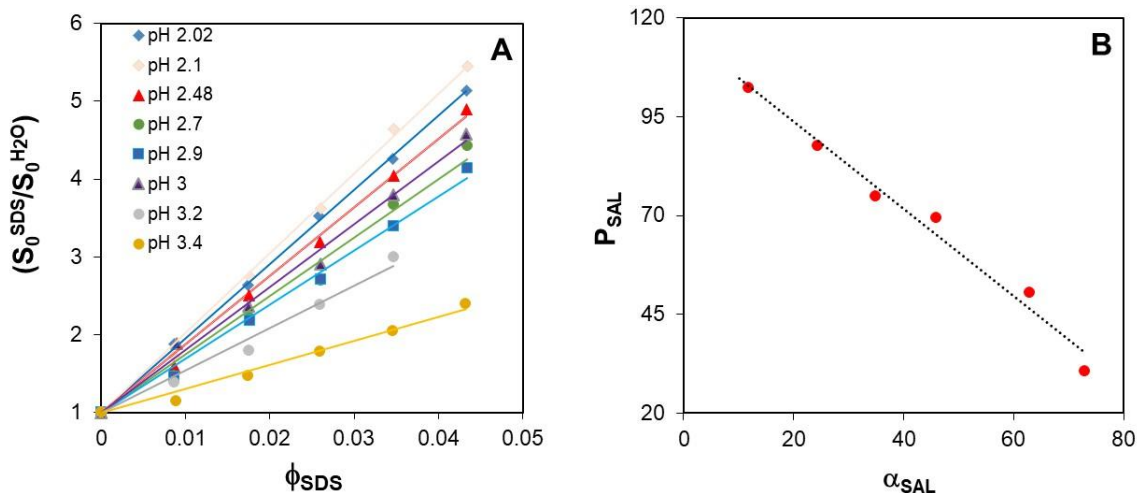
### 283 3. Results and Discussion

#### 284 3.1. Salicylic acid partition and binding constant to F127 micelles

285 Initially, the partition of SAL, both in molecular and ionized form, in F127 micelles, was  
286 determined from solubility data at 25°C in water and at different F127 concentrations, by  
287 UV-vis absorbance spectroscopy [48], over a range of pHs, therefore in systems  
288 containing varying fractions of ionized and unionized (“molecular”) SAL.

289 The solubility of SAL increases with F127 concentration at all pHs studied  
290 (supplementary material, SI 1).  $S_{0,F127}/S_{0,H2O}$ , at 5% F127, is higher at pH values below  
291 the pKa (pKa = 2.97 [49]), where the non-ionized form of the drug is present in higher  
292 amounts, in very good agreement with a higher solubilisation of the molecular form of the  
293 drug, rather than the charged (anionic one) in the micelles.

294 The solubility ratio  $S_{0,F127}/S_{0,H2O}$  increases linearly with the volumetric fraction of F127  
295 (Figure 1A). The slope of the curves increases as the pH decreases, reflecting a higher  
296 partitioning of the molecular vs. the ionized form present in the system at each pH. A  
297 linear fit of these plots at different values of the pH against the ionization percentage  
298 (Figure 1B) enables an extrapolation of the partition to 0% and 100% ionization,  
299 corresponding to the molecular and ionized forms of the drug, respectively. The results  
300 obtained are  $P = 115.7$ ,  $\log P = 2.1$  ( $\log P = 2.3$  in octanol/water [50]), for molecular SAL,  
301 and  $P = 5.5$ ,  $\log P = 0.74$ , for ionized SAL ( $P = -1.36$  in octanol/water [51]). A very good  
302 agreement of the molecular partition with that in octanol/water is found; in contrast, the  
303 partition of ionized SAL is much higher than in octanol/water. This effect has been  
304 recently observed in the case of naproxen loaded in SDS micelles (Valero 2020, under  
305 review). In both cases, despite the low dielectric constant of the environment, the presence  
306 of water in the micelles could facilitate partition compared to octanol. This result shows  
307 that F127 is able to efficiently load salicylic acid present at pH=1 in the stomach, in  
308 contrast to ionized salicylate, present at pH values above the pKa, which showed lower  
309 partition [18].



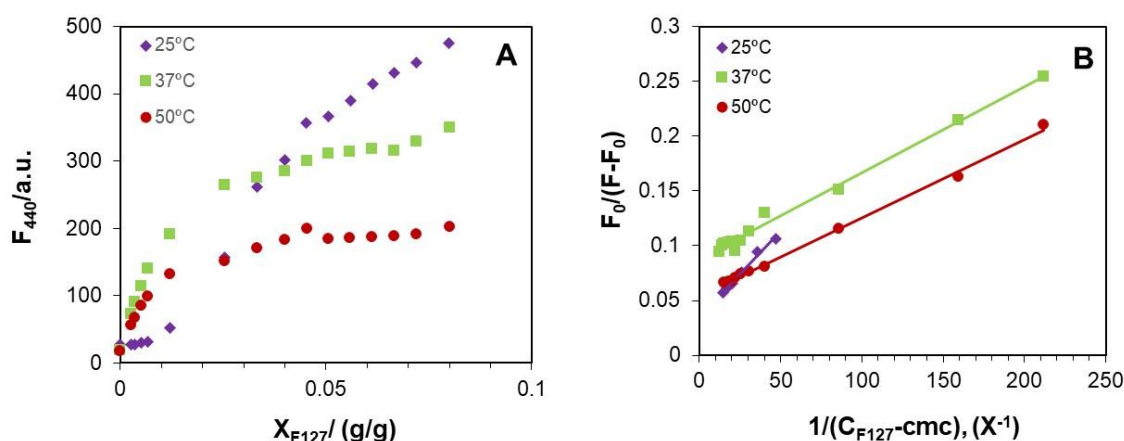
310

311 **Figure 1. A:** Change of SAL solubility with F127 volume fraction, at different values of  
 312 pH; **B:** SAL partition ( $P_{SAL}$ ) against ionization degree of SAL ( $\alpha_{SAL}$ ) in H<sub>2</sub>O at 25°C.

313

314 In order to compare the partitioning at pH=1 and pH=7, the binding constant of SAL to  
 315 F127 at pH=1 was also obtained by fluorescence spectroscopy, using a method previously  
 316 used for ionized salicylate as sodium salt [17,18]. In this case, the emission spectrum of  
 317 SAL in the presence of increasing amounts of F127 was obtained and the variation in  
 318 emission intensity ( $\lambda_{em}=440$  nm) with polymer concentration (Fig.2A) was fitted to Eq.  
 319 (1) (Fig.2B).

320 .



321

322 **Figure 2: A:** Change in fluorescence intensity at  $\lambda_{em}=440$  nm for 0.16 wt% SAL in H<sub>2</sub>O  
 323 in the presence of increasing amounts of F127, at 25° C (diamonds), 37° C (squares) and  
 324 50° C (circles). **B:** fitting of the data to Eq.(1).

325

326 The results shown in Table 1 show a higher partition at pH 1, compared to pH 7, despite  
 327 the higher drug concentration used (2% wt) at neutral pH compared to acidic pH (1 wt%).

pH	$K_{F127}/X^{-1}(g/g)/Diluted$			$K_{F127}/X^{-1}(g/g)/Concentrated$		
	298K	310K	323K	298K	310K	348K
1 (H <sub>2</sub> O)	7.4±0.07	77.6±0.15	110±0.51	71±0.07		
7 (H <sub>2</sub> O)	No detected*	No detected**		4.55±0.32*	18.3±0.3**	
1 (D <sub>2</sub> O)	10±0.41	107.5±0.25	74.3±0.52	78±0.30	116±0.36	79±4.58

328

\* data reproduced from [17]; \*\* data reproduced from [18].

329

330 **Table 1.** Binding constant  $K_{F127}$  (g/g) of sodium salicylate to 5 wt% F127 Pluronic  
 331 micellar solution in H<sub>2</sub>O and D<sub>2</sub>O at pH=1, at different temperatures, determined from the  
 332 variation of  $F_{440}$  with surfactant concentration using Eq (1). Two drug concentrations are  
 333 studied: diluted ( $C_{drug} = 1.5 \times 10^{-3}$  wt%) and concentrated ( $C_{drug} = 0.16$  wt%). For  
 334 comparative purposes, the results obtained in H<sub>2</sub>O at pH=7 are included; in this case SAL  
 concentrations were  $1.5 \times 10^{-3}$  wt% and 2 wt%.

335

336 The partition of molecular and ionized SAL obtained from absorption and emission  
337 spectra, at high drug concentration and 25°C, were compared. For this purpose, partition  
338 (P) was determined from the binding constant obtained from fluorescence using equation  
339 (2). The binding constant ( $K_{F127}$ ) of salicylate anion to F127 was found to be  $K_{F127} = 4.55$   
340  $X^{-1}$  ( $X^{-1}$ : inverse of concentration in g/g) [17] ( $K_{F127} = 56.8 M^{-1}$ ), which gives  $P = 6.3$  (log  
341  $P=0.80$ ) for the partition of the anionic form; this value is in very good agreement with  
342 the value of  $P=5.5$  (log  $P=0.74$ ) obtained by absorption spectroscopy. In the case of  
343 molecular SAL,  $K_{F127}=71 X^{-1}$  (Table 1) ( $K_{F127}= 886 M^{-1}$ ), which gives  $P = 83$  (log  $P=1.9$ ).  
344 The larger difference obtained for molecular salicylic acid partition ( $P = 83$  vs.  $P = 115.7$ )  
345 with both techniques, arises from the difference in the drug concentration used: in  
346 fluorescence, the working concentration of SAL is limited by its aqueous solubility,  
347 whereas in UV-vis absorbance it is the solubility in F127 micelles, hence the higher  
348 partition obtained by absorption can be attributed to the higher drug concentration, as  
349 usually observed [17,18,52,53].

350 Finally, and in order to reproduce the conditions used in the study of micellar morphology  
351 by SANS (see further down), the partition was also obtained in  $D_2O$ , at 25, 37, and 75 °C  
352 at both SAL concentrations. As can be observed (Table 1), partition is not affected by the  
353 solvent ( $H_2O$  vs  $D_2O$ ); it increases with temperature and drug concentration as observed  
354 in water [17,18,29,52,53].

355 Overall, the number of drug molecules inside the aggregate at pH=1 is much higher than  
356 at pH=7, in agreement with the absence of charge at low pH and the lower aqueous  
357 solubility. No major differences are observed in the partition of the drug in  $H_2O$  and  $D_2O$ .

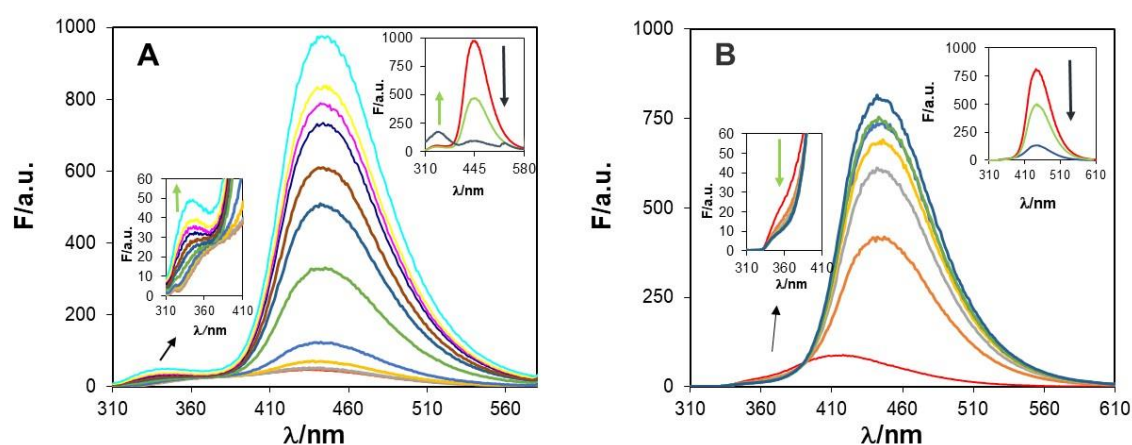
358 The emission spectrum of SAL is sensitive to changes in the properties of the environment  
359 in which it is solubilized [54–56]. These changes could provide valuable information  
360 about the local compartment where SAL is solubilized in the micelles, as well as the  
361 interaction of the drug with the aggregates. Therefore, in addition to partition, we next  
362 study the changes in fluorescence spectra of SAL in  $D_2O$  under different conditions.

363

### 364 3.2. Photophysical behavior of salicylic acid loaded in F127 micelles

365 SAL emission spectrum is known to show two bands, the band in the UV region is referred  
366 to as the U-band (appearing in the range  $\lambda_{max}=340 - 370$  nm), and the another in the blue  
367 region is known as the B band (appearing in the range  $\lambda_{max} = 380 - 480$  nm)[57]. SAL  
368 species emitting at each band could be different depending on the medium in which the  
369 drug is solubilized, in this case water or the micelle. Salicylic acid in polar solvents is  
370 present as different ionized species (monocation, monoanion and dianion), whereas in its  
371 non-polar form it dimerizes at moderate concentrations [56]. In addition, in the excited  
372 state, SAL undergoes intramolecular proton transfer (excited state intra-molecular proton  
373 transfer, ESIPT), between the carboxylic ketone and the adjacent hydroxyl group giving  
374 rise to a cycle. In general, non ESIPT species of SAL emit in the U band, whereas species  
375 undergoing ESIPT emit at B band. Depending on the emissive species present under  
376 different conditions, the emission spectra of the SAL, shape, intensity and maxima  
377 position, could be modified.

378 The emission spectrum of  $1.15 \times 10^{-3}$  wt % SAL in D<sub>2</sub>O (Fig 3A) shows a main band ( $\lambda_{\text{max}} =$   
 379 436 nm) and a shoulder ( $\lambda_{\text{max}} = 360$  nm); the main band is centered between that of the  
 380 monocation ( $\lambda_{\text{max}} = 407$  nm), expected to be present at the working pH, and the zwitterion  
 381 (ESIPT species) appearing in methanol at acidic pH ( $\lambda_{\text{max}} = 450$  nm) [55]; it suggests that  
 382 the spectrum corresponds to the emission of a mixture of both species: the monocation  
 383 emitting at a lower wavelength (U band) and the neutral SAL (ESIPT) emitting at high  
 384 wavelength (B band). At 0.16 wt % of SAL (Fig. 3B), a main band ( $\lambda_{\text{max}} = 415$  nm), with  
 385 a less pronounced shoulder is present in the spectrum. The position of the main band  
 386 ( $\lambda_{\text{max}} = 415$  nm) is also red-shifted compared to that of SAL as a monocation ( $\lambda_{\text{max}} = 407$   
 387 nm), suggesting the presence of some neutral form (ESIPT). The protonation equilibrium  
 388 seems to be shifted towards the neutral form in diluted system but towards the monocation  
 389 in the concentrated one, perhaps due to a lower pH produced by the presence of higher  
 390 amounts of SAL.  
 391



392  
 393 **Figure 3:** Emission spectra of SAL in the presence of increasing amounts of F127 (0-5  
 394 wt%) in D<sub>2</sub>O at different temperatures **A:** diluted  $1.5 \times 10^{-3}$  wt% SAL. **B:** concentrated  
 395 0.16 wt% SAL. *Insets left:* change in the emission intensity of U (340 nm) band with F127  
 396 concentration; *Insets right up:* fluorescence spectra of SAL loaded F127 micelle at 25°C  
 397 (brown), 37°C (green) and 75°C (blue).

398  
 399 The addition of F127 produces a strong increase in the emission intensity and a red shift  
 400 of the main band of the spectrum (Figure 3) from  $\lambda_{\text{max}} = 436$  or  $415$  nm in D<sub>2</sub>O (diluted  
 401 and concentrated SAL respectively) to  $\lambda_{\text{max}} = 445.5$  nm in F127 (B band), at both drug  
 402 concentrations. In general, shifts in the maximum of the bands of the spectra are related  
 403 to changes in the polarity of the local environment. In addition, the increase in the emission  
 404 intensity shows a decrease in deactivation processes of the excited state. Non-radiative  
 405 deactivation of SAL dissolved in polar alcoholic solvents decreases as the viscosity of the  
 406 alcohol increases [55]. Therefore, these changes show that SAL is transferred from the  
 407 polar D<sub>2</sub>O to the apolar micellar environment, in good agreement with SAL partition. The  
 408 maxima position shows that in the micelle the SAL is mainly in its neutral form  
 409 undergoing ESIPT ( $\lambda_{\text{max}} = 450$  nm) [55], at both drug concentrations.

410 At pH = 7, the maxima position ( $\lambda_{\text{max}} = 410$  nm [17]), appears strongly blue-shifted and  
 411 presents a higher emission intensity than in acidic conditions, characteristic features of the  
 412 deprotonated salicylate anion [57–59]. Partition of SAL in F127 micelles produces a

413 quenching of the fluorescence of the emission band [17], due to the proton transfer from  
414 the water to the ionized carboxylic hydroxyl group of the anionic SAL inside the micelle,  
415 as observed in a poly (vinyl alcohol) matrix [60] and in dioxane and acetonitrile water  
416 mixtures [58]. This behavior agrees with the increase in the emission intensity when SAL  
417 partitions at pH=1 and the existence of only the deprotonated ESIPT in the micelle.  
418 Inclusion in cationic micelles of cetyl (CTAB) [61] tetradecyl (TTAB) [59]  
419 trimethylammonium bromide produced an increase in the fluorescence in good agreement  
420 to non protonation of the salicylate due to the interaction with the positive charge of the  
421 surfactant, which produces a growth of the micelles [59,61] even in microemulsions [62].

422 The intensity of the B band decreases with temperature at both drug concentrations, (Fig.  
423 3A and B, *Insets right*), which shows temperature promotes some non-radiative  
424 deactivation mechanism. The vibrational deactivation of the excited state of the emissive  
425 species, due to a decrease in viscosity with temperature, is well known in homogeneous  
426 media [55]. In contrast to the homogeneous media, the micelle size increases with  
427 temperature [18], so the micelle inside is expected becomes more viscous.

428 By contrast to the B band, in the presence of F127, the U band, appearing in bulk D<sub>2</sub>O,  
429 undergoes different changes depending on drug concentration. At  $1.15 \times 10^{-3}$  wt% ( $\sim 10^{-4}$   
430 M) SAL concentration, its intensity increases with F127 concentration (Figure 3A, *Inset*  
431 *left*); hence, inside the micelles, there is a SAL species, without ESIPT, emitting at this  
432 band ( $\lambda_{\max} = 340$  nm). This emitting species is promoted by temperature, as this the main  
433 band at 75°C (Figure 3A, *Inset right*). The emitting species at the U band in non-polar  
434 media, it has been usually assigned to dimers without ESIPT [54,55,63,64]. However,  
435 dimers were detected in cyclohexene at drug concentration,  $10^{-5}$ M, lower than in the  
436 present case, the increase in temperature decreases the amount of dimers [56], so a  
437 decrease in the U band with temperature would be expected. Although the effect of  
438 temperature on the micelles could be different to homogeneous media, the presence of  
439 other species other than dimers must be consider (most probably, the cation detected in  
440 bulk D<sub>2</sub>O).

441 At higher SAL concentration, 0.16 wt % ( $1.16 \times 10^{-2}$ M), the intensity of the U band  
442 appearing in D<sub>2</sub>O (Figure 3B, *Inset left*) decreases as F127 concentration increases and  
443 SAL is transferred from water to the micelles, consequently, the emitting species without  
444 ESIPT, emitting at the U band, is not present when the drug is completely inside the  
445 micelle. The U band is not present in the micelle at any temperature studied at this drug  
446 concentration (Figure 3B, *Inset right*). Therefore, in the concentrated system, only the  
447 ESIPT emitting species exists. The same feature was described in the  $10^{-3}$ M SAL in a poly  
448 (methyl methacrylate) polymer matrix, PMMA. It was related to intermolecular hydrogen  
449 bonding of SAL, through the carboxylic hydroxyl group and the polymer [55] which  
450 strengthen the intramolecular one, ESIPT [54], promoting the species emitting at B band  
451 over the U one (assigned in this study to a dimer, the most expected species in non-polar  
452 media).

453 Since the photophysical behavior of SAL is governed by protonation, the behavior  
454 observed with drug concentration and temperature at pH=1 could be explained on the basis  
455 of different protonation of the carboxylic hydroxyl group. In the micelle, the same species  
456 are present, namely, the monocation and neutral form (ESIPT). The micelle is more  
457 efficient as a proton donor at low drug concentration (presence of U band) and at high

458 temperature (quenching of B band at both drug concentrations and in diluted systems the  
459 appearance of the U band).

460 Despite the micellar core location of the drug demonstrated before by NMR [18] and the  
461 possibility of forming inter-molecular hydrogen with PPO groups of F127 in the micelles  
462 as observed in mixtures of F127 with polyacids [25], the results point to a different  
463 hydration of the drug inside the micelles at the origin of the effects observed with  
464 concentration and temperature at pH=1, as reported recently for other compounds [65],  
465 as well as for the anionic salicylate in a poly (vinyl alcohol) matrix [60] and in mixtures  
466 of solvents with water [58]. In these studies, water clusters act as proton donors to the  
467 salicylate anion, resulting in a quenching of fluorescence. Interestingly, quenching of  
468 fluorescence produced by water was demonstrated to be dependent on the size of the water  
469 cluster, being operative at high water content ( $x_{H_2O} \geq 0.8$ ) in dioxane/water mixtures [58].

470 In order to obtain information about the water content in the free and loaded micelles, we  
471 next checked the polarity of the core of the aggregates by UV-absorption using Nile Red  
472 as a molecular probe.

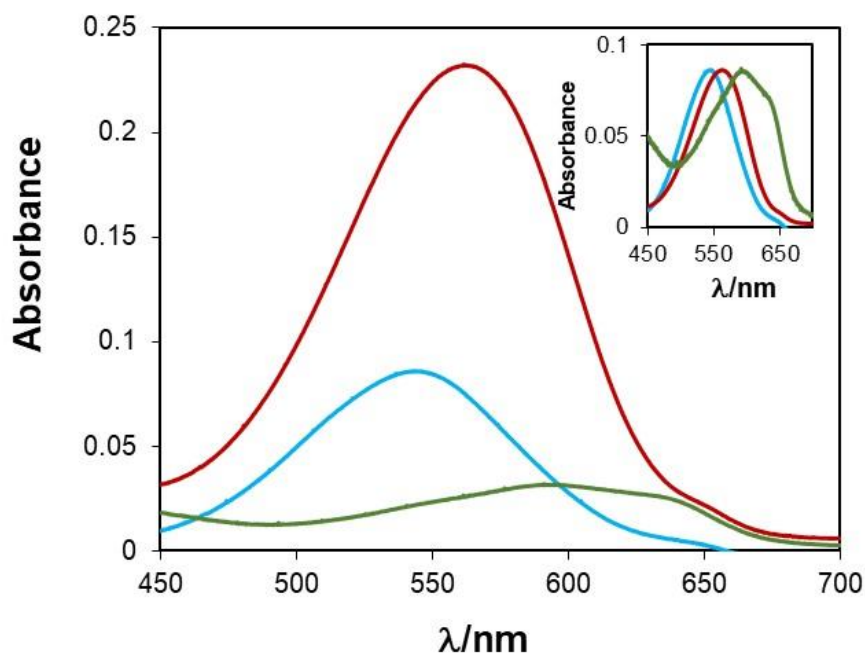
473

### 474 3.3. Nile Red as a probe of the polarity and water content of the micelles

475 Nile red (NR) is a fluorescent probe that presents a high sensitivity to the polarity of the  
476 medium [66–68] and therefore to the presence of water. The absorption and emission  
477 maxima of the probe are red-shifted when it is transferred from a non-polar to a polar  
478 medium [69,70]. NR and SAL absorption spectra do not overlap, making this probe a  
479 suitable candidate to examine the water content of the micellar region of the aggregate  
480 where it is located, in both the free and the SAL-loaded F127 micelles.

481 The absorption spectra of NR in H<sub>2</sub>O, 5 wt % F127 and SAL:F127 (1:5 wt%) at pH=1 are  
482 shown in Figure 4. In water, NR shows a low absorbance band centred at  $\lambda_{max}=594$  nm.  
483 The addition of F127, in both cases, produces a strong hyperchromic effect (Figure 4),  
484 besides a blue shift in the maximum  $\lambda_{max}=544$  nm and  $\lambda_{max}= 562$  nm in the absence and  
485 presence of SAL, respectively. These changes show that NR, in both cases, is being  
486 transferred from the bulk water to a less polar media, that is, inside the micelles. The  
487 strong red shift of the NR maximum position when partitioned inside the micelles, in the  
488 presence of drug, points to a higher polarity in SAL-loaded micelles than in the free  
489 micelles. Therefore, in contrast to what was speculated in the previous section, NR points  
490 to a higher water content of the SAL-loaded micelles than in the free micelles.

491



493

494

495

496

497

498

**Figure 4:** Nile Red  $4.66 \times 10^{-5} \text{M}$ : **A:** UV-vis absorption spectra in  $\text{H}_2\text{O}$  (green), 5% F127 (Blue) and SAL1% F127 5% (dark red),  $\text{pH}=1$ . *Inset:* Shift of these bands by manipulation of the bands to show them on a comparable scale (multiplying and dividing by 2.7, in water and SAL loaded system, respectively).

499

500

501

502

503

504

505

506

507

A rough estimation of the polarity of the microenvironment where the probe is dissolved can be obtained by comparing the maxima position of NR in the micelle to that in a medium of known dielectric constant. In the free micelles at  $\text{pH}=1$ ,  $\lambda_{\text{max}}=544 \text{ nm}$ , the polarity is between acetone ( $\epsilon=20.7$ ,  $\lambda_{\text{max}}=536 \text{ nm}$ ) and EtOH ( $\epsilon=24.5$ ,  $\lambda_{\text{max}}=554 \text{ nm}$ )[71], or between dichloromethanol ( $\epsilon=8.93$ ,  $\lambda_{\text{max}}=538 \text{ nm}$ ) and acetonitrile ( $\epsilon=37.5$ ,  $\lambda_{\text{max}}=556 \text{ nm}$ )[72]. Hence NR in the micelles would be in a medium with a dielectric constant around  $\epsilon=23$  (obtained as a mean value of the dielectric constants of homogeneous media with similar absorption maxima).

508

509

If we consider that only PPO or PEO and water are contributing to the polarity, the dielectric constant of the micellar core may be related to the water content by equation 5:

510

$$\epsilon = X_1 \times \epsilon_1 + X_{\text{H}_2\text{O}} \times \epsilon_{\text{H}_2\text{O}} \quad \text{Eq. 5}$$

511

512

513

514

where  $X_1$  is the fraction of PPO or PEO in the micelle, depending if the probe is in the core or the shell, respectively;  $\epsilon_1$ : is the dielectric constant of PPO or PEO depending if the probe is in the core or the shell, respectively. The dielectric constant of propylene oxide is  $\epsilon=16$  [73] and ethylene oxide  $\epsilon=13$  [74].

515

516

517

518

The water content obtained for the micellar compartment where the probe is located would be 11% (considering  $\epsilon$  of PPO and PEO, respectively). These values are far from the shell water content, which usually is higher than 90% [18], pointing to a core location of NR; the value of 11% is in very good agreement with the value of 10% reported for F127

519 micelles (3 %) [75], or 17% for 1% F127 at 37°C [42] and other Pluronics [76,77] obtained  
520 by SANS.

521 In the SAL-loaded micelles, NR absorption maximum is  $\lambda_{\max}= 562$  nm, suggesting a  
522 dielectric constant higher than in acetonitrile ( $\epsilon=37.5$ ,  $\lambda_{\max}=556$  nm) [72], which gives a  
523 water content as high as 33.5% for the locus of the probe in the loaded micelle. This value  
524 is higher than values usually detected, however, in certain cases the volume fraction of  
525 water in the core can be as much as 40%, for example in P85 at 50-60°C, obtained by  
526 SANS [76].

527 The higher water content in the loaded micelle suggests that SAL retains water, in good  
528 agreement with intermolecular hydrogen bond formation, as suggested by fluorescence,  
529 but with the water molecules instead of with the PPO groups of the F127 core. On the  
530 other hand, this value could be overestimated due to the increase of the polarity of the core  
531 due to the presence of SAL itself [27]; in this case, a third term - corresponding to the drug  
532 contribution - should be included in Eq. 6, resulting in a lower value of the water content,  
533 or it could be that the drug promotes NR solvation inside the micelles [78].

534 Next, the effect of the presence of molecular SAL on the structural features of the micellar  
535 aggregates was investigated by SANS.

536

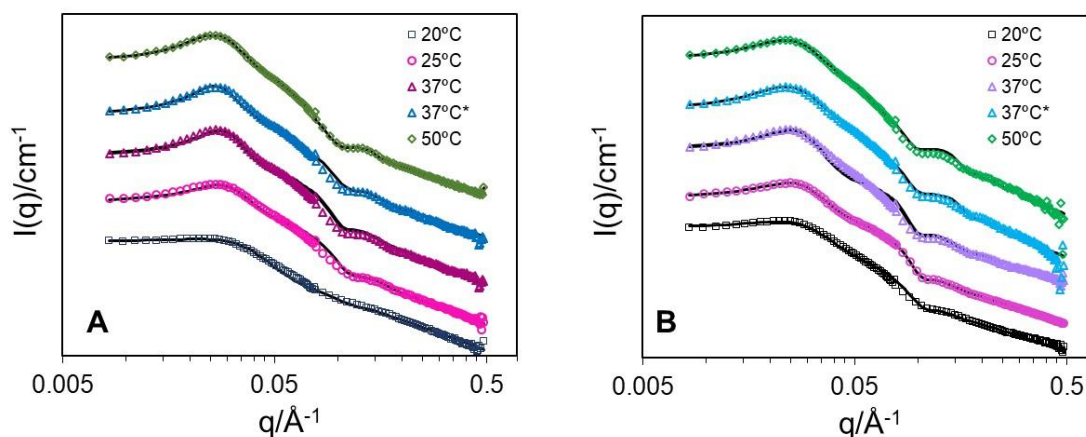
### 537 3.4. Small Angle Neutron Scattering of free and SAL-loaded F127 micelles

538 In this section, the effect of the presence of SAL on the micellar structure, with and without  
539 DIMEB, is examined at different temperatures.

540

#### 541 *3.4.1. Effect of acidic pH and temperature on F127 micelles*

542 SANS curves of free and SAL-loaded F127 micelles, at pH=1, were obtained over a range  
543 of temperatures (20 to 50°C) (SI 2) and fitted to different models (Figure 5).



544

545 **Figure 5:** Small-angle neutron scattering curves from A: free and B: SAL (1 wt%) loaded  
546 F127 (5 wt%) micelles at pH=1, at different temperatures, from 20 to 50 °C. The curves  
547 have been staggered for better visibility. Solid lines correspond to fits to CS-spheres (20-  
548 37 °C) or CS-cylinder (37 °C\*, 50 °C), combined with a hard sphere structure factor, at  
549 different temperatures.



550 The data were fitted by a core-shell sphere or cylinder model with a hard-sphere structure  
551 factor. The most important change in both free and loaded micelles is that temperature  
552 promotes the structuration of the micelles, with the reinforcement of the peak in the  
553 scattering curves, which reflects the presence of interactions. In addition, at high  
554 temperatures, we observed an elongation of the micelles (Tables 2, 3). At 20 and 25 °C,  
555 the curves are well described by a spherical core-shell model; at 37°C, they can be fitted  
556 both to spheres and cylindrical aggregates, with the latter giving better fits; at 50 °C, only  
557 the core-shell cylinder gives suitable fits, suggesting a transition from sphere to rods with  
558 temperature. The presence of SAL in the micelles seems to promote this elongation at  
559 lower temperature (37 °C), leading to longer micelles at 37 °C (151 vs. 106 Å in the  
560 absence of drug) (Tables 2, 3), and of similar length at 50 °C ( 153 vs. 150 Å) (Tables 2,  
561 3). Therefore, a combination of low pH, high temperature and presence of SAL seems to  
562 promote micellar growth. No data about the effect of acidity on free or loaded F127  
563 micelles was found in the literature. Micellar growth was not observed at neutral pH over  
564 the range 30-50 °C [79], or in the SAL-loaded micelles at 37 °C [18]. In agreement with  
565 these findings, paclitaxel, an anti-cancer drug, was found to induce micelle agglomeration  
566 and a shape transition of F127 to cylindrical micelles over the temperature range 37-50 °C  
567 [80]. In mixtures of F127 with poly (aspartic acid), the formation of cylindrical micelles  
568 was also suggested on the basis of viscosity measurements [25]. A sphere-to-rod transition  
569 of F127 has also been observed upon approaching the cloud point in the presence of NaCl  
570 and butan-1-ol [81]. Cylindrical micelle formation has also been described for smaller  
571 Pluronics such as P85 loaded with SAL at pH=1 [27], or P123 and P103 loaded with  
572 salicylic derivatives (methyl-salicylate and acetyl salicylic) at pH=7 [82], in both cases at  
573 25 °C. P105 loaded with glucose was also shown to form ellipsoid micelles at 55-60°C  
574 [83]. The origin of this shape transition is not clear; in some cases shell dehydration has  
575 been invoked [27,83,84], but in other studies micellar growth was assigned to core  
576 dehydration [81,82].

577

<b>T/°C</b>	<i>Core Radius Å</i>	<i>Shell Thickness Å</i>	<i>Length Å</i>	<i>Volume fraction</i>	<i>%D<sub>2</sub>O core</i>	<i>%D<sub>2</sub>O shell</i>
<b>20</b>	34	47	-----	0.12	41	94
<b>25</b>	37	61	-----	0.22	0	94
<b>37</b>	40	65	-----	0.29	0	92
<b>37*</b>	34	52	106	0.29	17	94
<b>50</b>	36	44	150	0.25	23	93
<b>25</b>	40	58	-----	0.14	0	90
<b>37<sup>a</sup></b>	45	64	-----	0.25	0	92

578 <sup>a</sup> data reproduced from [18]

579 **Table 2:** Fitting parameters obtained from SANS curves of F127 micelles (5  
580 wt%) at pH=1 in D<sub>2</sub>O described by CS-spheres (20-37 °C) or CS-cylinders  
581 (37\*, 50 °C), combined with a hard-sphere structure factor, at different

582 temperatures. For comparison, the last two rows include the data collected at  
 583 pH=7, at 25 and 37 °C <sup>a</sup>, fitted to CS-spheres with a hard-sphere structure  
 584 factor.

585

T/°C	Core Radius Å	Shell Thickness Å	Length Å	Volume fraction	%D <sub>2</sub> O core	%D <sub>2</sub> O shell
20	39	61	-----	0.13	0	94
25	40	65	-----	0.20	0	94
37	43	66	-----	0.27	0	90
37*	38	48	151	0.28	33	94
50	39	45	153	0.26	35	92
25 <sup>a</sup>	35	52	-----	0.13	0	96
37 <sup>a</sup>	41	64	-----	0.26	0	92

586 <sup>a</sup> data reproduced from [18]

587 **Table 3.** Fitting parameters obtained from SANS curves of F127 micelles (5  
 588 wt%) loaded with SAL (1 wt%) at pH=1 in D<sub>2</sub>O described by CS-spheres (20-  
 589 37 °C) or CS-cylinders (37\*, 50 °C), with a hard-sphere structure factor, at  
 590 different temperatures. For comparison, the last two rows include the data  
 591 collected at pH=7, at 25 and 37 °C <sup>a</sup>, fitted to CS-spheres with a hard-sphere  
 592 structure factor.

593

594 We next turn our attention to the water content in the two compartments [85] of the  
 595 micelles (core and shell). First, the shell of both free and SAL loaded micelles is highly  
 596 hydrated (Tables 2 and 3), as observed for Pluronics and other PEG-base copolymers  
 597 [18,85]. No meaningful change in the water content of the shell is observed with  
 598 temperature (94% at 20°C and 93 - 92%, at 50°C), the presence of SAL (94% at 37°C for  
 599 both systems or 93- 92% for free and SAL loaded aggregates, respectively at 50°C) or  
 600 with pH (free micelles: at 25°C 94/90% and at 37°C 94/92% at pH=1/pH=7; or in the  
 601 loaded micelles: 94/96% and 94/92% at 25 and 37°C, pH=1/pH=7, respectively). This  
 602 would suggest that hydration of the shell is unlikely to be playing a key role in micellar  
 603 growth; however neutrons are not very sensitive to this region of the micelles (in particular  
 604 to the chains further away from the aggregates).

605 In order to minimize the number of floating parameters, and based on previous studies of  
 606 similar polymers [18,85], the water content of the core was initially fixed to zero, in other  
 607 words, the scattering length density was fixed to the value of PPO ( $0.4 \times 10^{-6} \text{ \AA}^{-2}$ ).  
 608 However, this assumption does not allow the fitting of the curves at all temperatures. In  
 609 the free micelles, at 20°C, the amount of water in the core was found to be quite high  
 610 (41%), a value that is in good agreement with reported values of 37% or 40% for P123 in  
 611 D<sub>2</sub>O with 1.6M HCl at this temperature [77]; the water content is known to increase as  
 612 temperature decreases [86] due to the higher polymer solubility and the formation of large

613 pre-aggregates [87]. In contrast to the free micelles, at this temperature (20°C), SAL-  
614 loaded micelles can be fitted by considering a fully dehydrated core, suggesting that the  
615 micelle are fully formed (not pre-aggregates), suggesting that the presence of drug  
616 promotes micelle formation at lower temperatures. At 25 °C, the curves of free and SAL-  
617 loaded micelles could all be fitted without water in their core. However, at 37° and 50°C,  
618 when cylindrical micelles are formed, the presence of water in the core needs to be  
619 accounted for in all the micellar systems studied. In order to check the water content, the  
620 values obtained for the cylindrical micelles model were used. In free 5% F127 micelles,  
621 we obtained 17 and 23 % at 37 °C and 50 °C, respectively. These values are in good  
622 agreement with the value of 11% found for the free micelles at 25 °C with the NR (previous  
623 section) and 17% obtained for 1 wt% F127 micelles at 37°C [42], or around 20% for P123  
624 micelles at 40°C [77].

625 In the presence of SAL, the water content in the core is double that of the free aggregates:  
626 33 and 35% at 37 and 50 °C, respectively. The value at 37 °C is in very good agreement  
627 to the one obtained by fluorescence with NR at 25°C, reinforcing the idea of water  
628 retention by the drug and strong hydration of SAL in the aggregates' core. The water  
629 content of the core tends to increase with an increase in temperature in the free and SAL-  
630 loaded micelles; this effect was not observed with P123 in HCl [77]. On the other hand,  
631 EO groups tend to associate to protonated water molecules ( $H_3O^+$ ) through the ether group  
632 [87]. Hydrogen bond formation between polyacids and ether groups, both with the PEO  
633 and PPO blocks of F127, has also been demonstrated [88]. Hence the protonation of the  
634 polymer chains and the presence of SAL seem to promote the presence of more water  
635 molecules in the aggregates as temperature increases.

636 Overall, therefore, core dehydration does not seem to be a driving force for micellar  
637 growth, since hydration seems to increase with temperature. What is changing in the  
638 systems under these conditions?. Looking at the features of free and SAL-loaded F127  
639 micelles at pH=1 (Tables 2, 3), it is possible to make three observations. First, we observe  
640 the size of the core slightly increases with temperature. In the presence of SAL, the core  
641 is slightly swollen compared to the free micelles, at all temperatures, in agreement with  
642 the core location of the drug [18], as observed with other anti-inflammatory drugs [26,89].  
643 Second, if we observe the thickness of the shell, this value increases with temperature in  
644 spherical micelles (47 to 65 Å or 61 to 66 Å in free and loaded micelles, from 20 to 37°C),  
645 then drops sharply with the transition to cylinders and decreases with temperature as  
646 cylindrical micelles grow (from 61 to 44 Å (F127) and 65 to 45 Å (SAL:F127), from 25°  
647 to 50°C, respectively).

648 Overall therefore, the data show that when the micelles grow (pH=1, T=37 and 50°C the  
649 shell shrinks slightly, and the core accommodates higher amounts of water, which would  
650 result in more space between the hydrophobic chains. In summary, at pH=1 and high  
651 temperature, free and SAL-loaded micelles form highly hydrated cylindrical micelles.

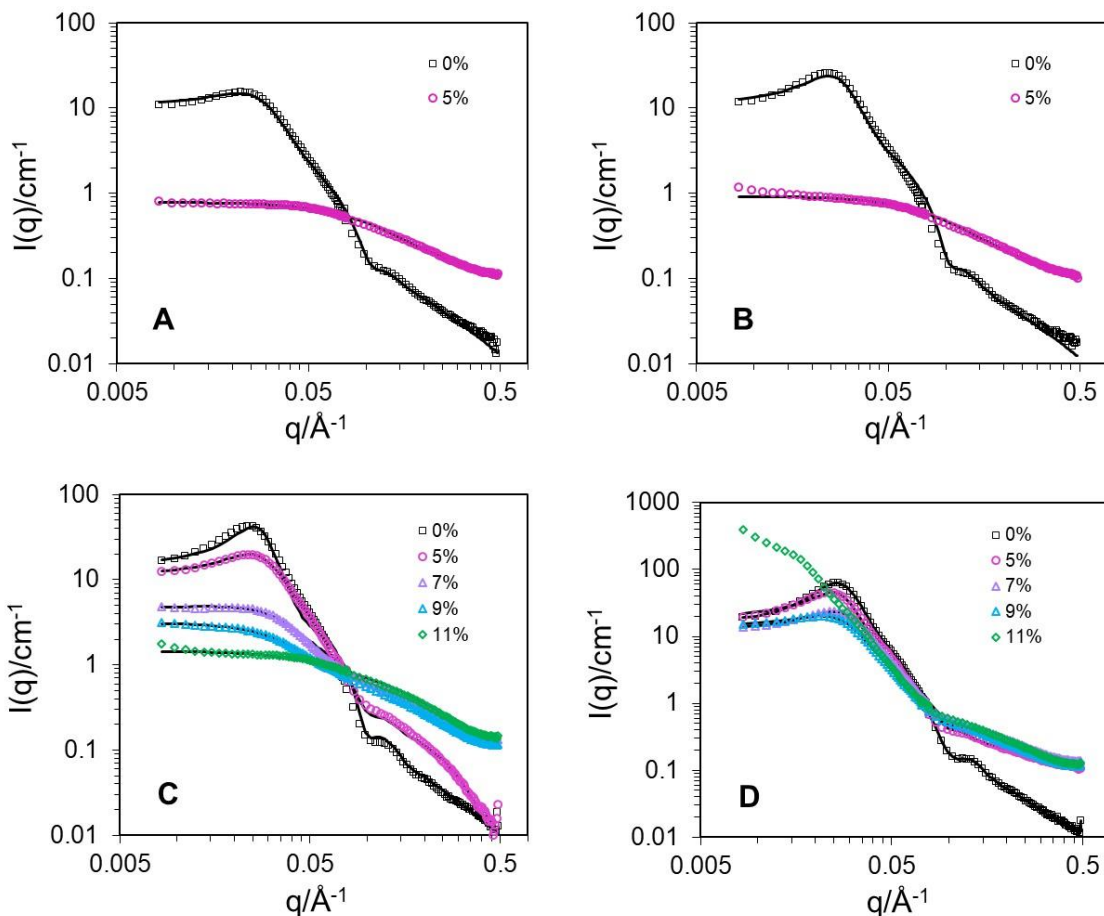
652 Next, we check whether SAL-loaded F127 micelles are protected against the disruptive  
653 effect of DIMEB at pH=1, in such a way that the drug could remain encapsulated in the  
654 micelles under gastric conditions.

655

656 *3.4.2. Interaction of SAL-loaded aggregates with DIMEB*

657 SANS curves were obtained in the presence of 5, 7, 9 and 11 wt% of DIMEB at 20, 25,  
 658 37 and 50 °C (Figure 6).

659  
 660



661  
 662 **Figure 6:** Small-angle neutron scattering curves of SAL (1%)-loaded F127 (5%) micelles  
 663 at pH=1 in the absence ( $\square$ ) and presence of 5% ( $\circ$ ), 7% ( $\triangle$ ), 9% ( $\triangle$ ) and 11% ( $\diamond$ ) of  
 664 DIMEB **A:** 20 °C; **B:** 25°C; **C:** 37 °C; and **D:** 50°C.

665  
 666 At 20 °C (Figure 6A) and 25°C (Figure 6B), the scattering curves are well fitted to  
 667 Gaussian coils (fitting parameters included in SI 3) at the lowest concentration of DIMEB  
 668 (5wt%), showing that SAL-loaded micelles are completely broken-up by the addition of  
 669 5 wt% DIMEB. At pH=7 and 25°C (SI 3 and 4), the same amount of DIMEB is necessary  
 670 to break up of the SAL-loaded micelles. In this case, salicylate partition is very low at this  
 671 temperature and the presence of the charged drug reduces the size of the aggregates [17].  
 672 The fact that SAL-loaded micelles are not protected against the action of DIMEB with  
 673 the high partitioning is observed (Section 3.1.) is unexpected, since in our previous [16–  
 674 18] of drugs has been found to afford some protection against the disruptive effect of  
 675 DIMEB. Hence, on the basis of the high SAL partitioning in the micelle core, a stronger  
 676 protective effect was expected compared to ionized SAL [17,18].

677

[DIMEB] wt %	Core Radius	Shell Thickness	Volume fraction	Shell sld ( $\times 10^6$ )/ $\text{\AA}^2$
-----------------	----------------	--------------------	--------------------	--

	Å	Å		
<b>5</b>	42	60	0.160	6.00
<b>7</b>	37	54	0.049	6.23
<b>9</b>	32	45	0.020	6.01
<b>9*</b>	35	57		6.17
<b>13*</b>	24	35		6.15
	<i>Scale</i>	<i>Rg/Å</i>		
<b>11</b>	0.29	26		

\* data taken from [18]

**Table 4.** Fitting parameters obtained from SANS curves of SAL (1 wt%)-loaded F127 micelles (5 wt%) at pH=1 in D<sub>2</sub>O at 37°C with a CS-spheres model in the presence of varying amounts of DIMEB. 9\*, 13\*: fits to the curves at pH=7.

678  
679  
680  
681  
682  
683  
684

685 Interestingly, at 37°C and 50 °C, the data could be fitted with spherical micelles, rather  
686 than cylindrical ones, from the lowest concentration of DIMEB (5 wt%). At 37°C, the size  
687 of the aggregates (Figure 6C, Table 5) decreases from 101 to 77 Å, as DIMEB  
688 concentration increases from 5 to 9 wt%; the volume fraction of the micelles also  
689 decreases concomitantly, from 0.160 in the absence of DIMEB up to 0.02, at 9 wt%  
690 DIMEB; at 11 wt% the micelles are fully broken up and the data can be fitted to Gaussian  
691 coils. Instead, at 50°C (Figure 6D, Table 5), the micelles also shrink from 112 to 101 Å  
692 with 5 and 7 wt% DIMEB, and maintain a constant size (102 Å) at 9 wt% and at 11 wt%  
693 DIMEB. Therefore temperature makes the micelle more stable against DIMEB disruption,  
694 as had been observed at pH=7 [17,18].

695 At both temperatures, it is possible to observe an excess intensity at low  $q$ , more  
696 pronounced at 50°C, possibly denoting the presence of larger structures [90,91].

697 In summary, the loaded micelles become more stable against DIMEB disruption as  
698 temperature increases, as observed for the free and SAL-loaded micelles at pH=7 (no data  
699 of free micelle at pH=1 is available). The effect of the temperature on the DIMEB  
700 disrupting ability has not been studied in depth, but it seems to be related the ability of the  
701 DIMEB to get in contact to the core [18]. Taking into account at pH=1 the water content  
702 increases with temperature this result suggests the water molecules inside the micelle  
703 package tighter as temperature increases making DIMEB diffusion, and therefore the  
704 breaking up, more difficult.

705

<b>%DIMEB</b>	<i>Radius</i> Å	<i>Thickness</i> Å	<i>Volume</i> <i>fraction</i>	<i>Shell sld</i> (10 <sup>6</sup> )/1/Å <sup>2</sup>
<b>5</b>	48	64	0.225	6.0
<b>7</b>	41	60	0.166	6.1
<b>9</b>	41	61	0.134	6.1

706

707 **Table 5.** Fitting parameters obtained from SANS curves of SAL (1 wt%)-loaded F127  
 708 micelles (5 wt%) at pH=1 in D<sub>2</sub>O at 50°C.

709

710

711 The effect of pH can be assessed by comparing micellar size in the presence of DIMEB at  
 712 pH=1 and 7. Ionized SAL-loaded micelles (pH=7), in the presence of 9 wt% DIMEB,  
 713 present the same size (92 Å [18]) as the molecular SAL-loaded micelles (pH=1) with 7%  
 714 DIMEB (91 Å, Table 4), and clearly higher than with 9% DIMEB (77 Å, Table 4) at  
 715 pH=1. With 13 % DIMEB at pH=7, small micelles (59 Å) are still present whereas at  
 716 pH=1 they are fully broken up with 11 wt% DIMEB.

717 For intestine-controlled release, SAL formulation should have a DIMEB concentration  
 718 higher than 13% (DIEMB concentration which completely breaks up the loaded micelle  
 719 at pH=7) [18]; but the present results show that at this DIMEB concentration, the micelles  
 720 would be broken up in the stomach releasing the loaded SAL and therefore not avoiding  
 721 the side effect of the drug which preclude oral administration of the drug.

722 In order to obtain further information about the disruptive effect of DIMEB, and assess  
 723 whether the lower competition of SAL with F127 for DIMEB contributes to the non  
 724 protective effect [18,90], the binding constant of molecular SAL (pH=1) to DIMEB,  
 725  $K_{\text{DIMEB}}$ , at 25 and 37°C, was determined in H<sub>2</sub>O and D<sub>2</sub>O (SI5). Binding constants  $K_{\text{DIMEB}}$   
 726 = 483 g/g (25°C) and  $K_{\text{DIMEB}}$  = 438 g/g (37°C) were obtained at pH=1. No difference in  
 727 the binding ability was found in D<sub>2</sub>O at pH=1. The binding constants at pH=1 are of the  
 728 same order as at pH=7,  $K_{\text{DIMEB}}$  = 440.9 g/g (25°C) [17] and  $K_{\text{DIMEB}}$  = 423.3 g/g (37°C)  
 729 [18]. In contrast, using potentiometry, a much larger difference in the complexation ability  
 730 between molecular SAL,  $K_{\text{DIMEB}}$  = 1570 M<sup>-1</sup>, and ionized SAL,  $K_{\text{DIMEB}}$  = 140 M<sup>-1</sup> with  
 731 DIMEB had been reported [92], contrasting with our data. If we indeed assumed a larger  
 732 DIMEB-SAL binding at pH=1, the free DIMEB available to interact with F127 micelles  
 733 would be lower at pH=1 than pH=7, which would contribute to protect the micelles, not  
 734 make it more susceptible to disruption as observed here.

735 Overall, we find that micelles at pH=1, with a high load of molecular SAL, are more  
 736 susceptible to disruption by DIMEB than at pH=7 (where a very low amount of SAL  
 737 partitions). Therefore, in a ternary formulation, the load would be released in the stomach.  
 738 However, on the basis of partitioning, F127 micelles can efficiently solubilize SAL, retain  
 739 it in the stomach and release it in the intestine, triggered by a change at physiological pH  
 740 without DIMEB involvement. This effect has also been observed in P104 loaded with  
 741 drugs with acid-basic properties [93], and it would be expected for SAL in P85 [27]. In  
 742 comparison however, Pluronic F127 shows a higher solubilization ability (>19  
 743 molecules/micelle, estimated from solubility data) than P85 (8 molecules/micelle) [27]. In  
 744 addition, the lower cmc of F127 (2.8×10<sup>-6</sup>M) compared to P85 (6.5×10<sup>-5</sup>M) reported [8]  
 745 makes the micelle less susceptible to dilution effects in the body. In addition, the ability  
 746 of F127 to form gels (at higher concentrations) make it a more attractive formulation for  
 747 SAL (and other drugs with gastro intestinal side effects).

748 From a mechanistic point of view, previous time-resolved SANS and NMR studies have  
 749 suggested that the interaction between the methyl groups of DIMEB and PPO may be  
 750 responsible for the instantaneous break-up of the micelles [94], and that drugs loaded  
 751 within the micelles (in addition to their ability to bind to DIMEB through inclusion  
 752 complexes) may modulate the interactions between DIMEB and the PPO blocks [18], in  
 753 particular by preventing interactions between DIMEB and PO units [16,18]. Sodium  
 754 salicylate partitions very weakly inside the micelles (Table 1) and its location could not  
 755 be determined by 2D NOESY NMR, whereas salicylic acid (in unionized form) is clearly  
 756 located in the core [18], and in high quantities (as reflected by a high partition coefficient  
 757 described in the present work). It is therefore all the more surprising that salicylic acid  
 758 provides less protection against micellar disruption by DIMEB than salicylate anions.

759 All these results taken together suggest that the high hydration of the SAL-loaded micellar  
 760 core, together with a higher separation between the polymer chains in the core to  
 761 accommodate water, compared to pH=7 at a given temperature, may favor the diffusion  
 762 of DIMEB through the micellar core and hence its interaction with PPO, which would  
 763 therefore support the proposed mechanism DIMEB-triggered mechanism of disruption.

764

### 765 3.5. Cloud Point (CP) determination

766 The solubility of triblock co-polymers decreases with temperature, because water  
 767 becomes a poorer solvent for PPO and PEO [95], ultimately leading to phase separation,  
 768 or a cloud point, at high temperatures. Therefore, the cloud point is an easily measurable  
 769 property of polymeric micelles sensitive to water content. For this reason, the cloud point  
 770 of F127 (5wt %) in D<sub>2</sub>O, free and loaded with SAL, was determined at pH=1 and pH=7  
 771 (Table 6).

772

System/D <sub>2</sub> O	CP		CP/ NaCl 2M/ D <sub>2</sub> O	
	pH=7	pH=1	pH=7	pH=1
<b>F127</b>	>98	>98	59	64
<b>SAL 1%</b>	>98	81	50	46-47
<b>SAL1%/H<sub>2</sub>O</b>		87		

773

774 **Table 6.** Cloud point of F127 (5 wt%), free and with 1 wt%  
 775 SAL at pH=1 and pH=7, in D<sub>2</sub>O in the absence and presence  
 776 of 2M NaCl. The cloud point for SAL-loaded micelles at  
 777 pH=1 in H<sub>2</sub>O is also included.

778

779

780 Free F127 micelles at pH=1 and pH=7, and SAL-loaded micelles at pH=7, all present a  
 781 CP above 98°C (the highest temperature measured). In contrast, in the presence of  
 782 molecular SAL (pH=1), the CP drops to 81°C (87 °C in H<sub>2</sub>O). The same effect was  
 783 described for SAL on the CP of P85 micelles [27]. A decrease in CP is generally attributed  
 784 to micellar dehydration [27,29,81] and an increase to micelle hydration [27,95], usually

785 in the region of the shell rather than the core [27], leading even to complete PEO  
786 dehydration [96].

787 In order to compare the CP of free and SAL-loaded F127 micelles at pH=1 and pH=7, the  
788 CP was shifted to lower temperatures by the addition of 2M NaCl. The CP of the free  
789 micelles at pH=7 (62°C) is in agreement with the value previously reported under the same  
790 conditions [29]. As can be observed in Table 6, the CP of free F127 micelles at pH=1 is  
791 slightly higher than at pH=7, which is attributed to the salting-in effect of hydrogen ions  
792 in non-ionic surfactants [97,98]. This behavior is in good agreement with a higher micellar  
793 hydration at pH=1. However, despite similar values of shell hydration observed for free  
794 and loaded micelles at 50 °C (Tables 2,3), and the higher water content of the core in the  
795 loaded micelles, the presence of SAL at pH=1 produces an effect opposite to predictions  
796 in decreasing the CP. The decrease of the CP produced by the addition of salts has been  
797 explained by the strong solvation of salts, which act “*as a pump*” to dehydrate the PEO  
798 [29], decreasing the solubility of the polymer and then its CP [29]. Therefore, given that  
799 the drug in its molecular form seems to bind strongly with the water molecules in the  
800 micelle, it is possible to speculate that it makes the polymer chains in the core less solvated  
801 than in its absence, despite the higher water content of the core in the loaded micelle. This  
802 behavior suggests the loaded aggregates need more water to be solubilized than the free  
803 ones, so when the micelle is not able to retain enough water the phase separation occurs,  
804 thus lowering the CP.

805 Surprisingly, the presence of SAL in ionized form also decreases the CP compared to free  
806 F127. This result is in good agreement to the decrease produced by ionized  
807 hydrochlorothiazide, CP=51 °C (which has a very different structure than SAL), in the  
808 presence of 2M of NaCl [29]. However salicylate increased the CP of P85, in the absence  
809 of NaCl [27]. It is worthy to note that in these conditions the effect produced by molecular  
810 SAL and ionized SAL is nearly the same, unlike in the absence of salt. So, in these  
811 conditions the system becomes very complex and a more detailed study would required.

812 While the characterization of the behavior of the water pools inside the micelles is not an  
813 easy task, these results give support to the idea that water has a fundamental role in all  
814 the processes that sustain micellar behavior, including drug solubilisation and release, and  
815 interactions with a third compound, as DIMEB in this study.

816

#### 817 **4. Conclusion**

818 F127 strongly increases the aqueous solubility of salicylic acid (SAL). SAL partitions  
819 significantly more in F127 micelles at pH=1 compared to pH=7, due to the absence of  
820 charge on the drug. The photophysical behavior of SAL reveals that the drug in the  
821 micelles forms intermolecular hydrogen bonds, possibly with F127, however further  
822 spectroscopy results suggest that it may instead be with water molecules. Quenching of  
823 SAL fluorescence inside the micelles is observed with increasing temperature,  
824 demonstrating that the vibration of the polymer chain forming the micellar core (where  
825 SAL is solubilized) increases with temperature. Nile red fluorescence shows that SAL-  
826 loaded micelles are more hydrated than the free micelles, with 30 and 17% of water in the  
827 core, respectively. SANS data analysis suggests that cylindrical micelles are formed at  
828 temperatures above 37°C, whose core seems to be more hydrated than at lower



829 temperatures: (17 vs 23 % and 33 vs 35% at 37 °C vs 50 °C for free and SAL-loaded F127  
830 micelles, respectively). The rearrangement of the water is suggested to be the main driving  
831 force for the sphere-to-cylinder shape transition. Despite the high amount of SAL  
832 molecules in the core, their presence does not afford protection to the micelles against  
833 disruption by DIMEB. In this case, the increased water content is likely to promote  
834 DIMEB diffusion, making interaction with the PO units in the core easier, which is one of  
835 the suggested mechanisms of micellar disruption. The presence of salicylic acid strongly  
836 decreases the CP of the loaded aggregate, which allows us to speculate that SAL indeed  
837 strongly binds the water molecules in the micellar core, decreasing PPO hydration.

838 From a practical point of view, F127 micelles are an efficient carrier of large amounts of  
839 drug; in addition, they can provide controlled intestinal release triggered by physiological  
840 changes in pH experienced by drugs after oral administration.

841 All the data taken together suggest that the water content is key to the re-arrangement of  
842 the polymer chains in the core of the aggregates, giving rise to a change in micellar  
843 morphology and also affecting the interaction of DIMEB with the micellar core, therefore  
844 facilitating the disruptive action of the cyclodextrins, and thus a controlled release  
845 mediated by this interaction. Overall, our results provide precious insights into the  
846 molecular interactions regulating drug loading and release in micellar nanocarriers and in  
847 more complex (ternary) systems, which provide a basis to rationalize formulation design.

848

#### 849 **Acknowledgements**

850 This work is based upon experiments performed at the KWS-2 instrument operated by  
851 JCNS at the Heinz Maier-Leibnitz Zentrum (MLZ), Garching, Germany. This work  
852 benefited from the use of the SasView application, originally developed under NSF Award  
853 DMR- 0520547. SasView also contains code developed with funding from the EU  
854 Horizon 2020 programme under the SINE2020 project. Grant No 654000.

855

856

#### 857 **References**

858

- 859 [1] A.M. Bodratti, P. Alexandridis, Formulation of poloxamers for drug delivery, *J.*  
860 *Funct. Biomater.* 9 (2018). <https://doi.org/10.3390/jfb9010011>.
- 861 [2] A.R. Fares, A.N. Elmeshad, M.A.A. Kassem, Enhancement of dissolution and  
862 oral bioavailability of lacidipine via pluronic P123 / F127 mixed polymeric  
863 micelles : formulation , optimization using central composite design and in vivo  
864 bioavailability study, 7544 (2018).  
865 <https://doi.org/10.1080/10717544.2017.1419512>.
- 866 [3] H. Shen, S. Liu, Enhancement of oral bioavailability of magnolol by  
867 encapsulation in mixed micelles containing pluronic F127 and L61, 70 (2018)  
868 498–506. <https://doi.org/10.1111/jphp.12887>.
- 869 [4] X. Wu, W. Ge, T. Shao, W. Wu, J. Hou, L. Cui, J. Wang, Z. Zhang, Enhancing  
870 the oral bioavailability of biochanin A by encapsulation in mixed micelles  
871 containing Pluronic F127 and Plasdane S630, *Int. J. Nanomedicine.* (2017) 1475–  
872 1483. <https://doi.org/http://dx.doi.org/10.2147/IJN.S125041>.
- 873 [5] Z. Zhang, C. Cui, F. Wei, H. Lv, Improved solubility and oral bioavailability of  
874 apigenin via Soluplus / Pluronic F127 binary mixed micelles system, 9045 (2017).

- 875 <https://doi.org/10.1080/03639045.2017.1313857>.
- 876 [6] E. V Batrakova, A. V Kabanov, Pluronic block copolymers : Evolution of drug  
877 delivery concept from inert nanocarriers to biological response modifiers, *J.*  
878 *Control. Release.* 130 (2008) 98–106.  
879 <https://doi.org/10.1016/j.jconrel.2008.04.013>.
- 880 [7] M. Agafonov, T. Volkova, R. Kumeev, E. Chibunova, I. Terekhova, Impact of  
881 pluronic F127 on aqueous solubility and membrane permeability of antirheumatic  
882 compounds of different structure and polarity, *J. Mol. Liq.* 274 (2019) 770–777.  
883 <https://doi.org/https://doi.org/10.1016/j.molliq.2018.11.060>.
- 884 [8] A. V. Kabanov, E. V. Batrakova, V.Y. Alakhov, Pluronic block copolymers as  
885 novel polymer therapeutics for drug and gene delivery, *J. Control. Release.* 82  
886 (2002) 189–212. [https://doi.org/DOI: 10.1016/s0168-3659\(02\)00009-3](https://doi.org/DOI:10.1016/s0168-3659(02)00009-3).
- 887 [9] Y. Guan, J. Huang, L. Zuo, J. Xu, L. Si, J. Qiu, G. Li, Effect of Pluronic P123 and  
888 F127 Block Copolymer on P-glycoprotein Transport and CYP3A Metabolism, 34  
889 (2011) 1719–1728. <https://doi.org/10.1007/s12272-011-1016-0>.
- 890 [10] Z. Wei, S. Yuan, J. Hao, X. Fang, Mechanism of inhibition of P-glycoprotein  
891 mediated efflux by Pluronic P123/F127 block copolymers: Relationship between  
892 copolymer concentration and inhibitory activity, *Eur. J. Pharm. Biopharm.* 83  
893 (2013) 266–274. <https://doi.org/10.1016/j.ejpb.2012.09.014>.
- 894 [11] M.S.H. Akash, K. Rehman, S. Chen, Pluronic F127-based thermosensitive gels  
895 for delivery of therapeutic proteins and peptides, *Polym. Rev.* 54 (2014) 573–597.  
896 <https://doi.org/10.1080/15583724.2014.927885>.
- 897 [12] C.-C. Pai-Chie, F. Sylvan G, In vitro release of lidocaine from pluronic F-127  
898 gels, *Int. J. Pharm.* 8 (1981) 89–99. [https://doi.org/10.1016/0378-5173\(81\)90013-](https://doi.org/10.1016/0378-5173(81)90013-2)  
899 [2](https://doi.org/10.1016/0378-5173(81)90013-2).
- 900 [13] S. Demirci, E. Karaku, Z. Hal, A. Topçu, Boron and Poloxamer ( F68 and F127 )  
901 Containing Hydrogel Formulation for Burn Wound Healing, (2015) 169–180.  
902 <https://doi.org/10.1007/s12011-015-0338-z>.
- 903 [14] C. Di Donato, R. Iacovino, C. Isernia, G. Malgieri, A. Varela-garcia, A.  
904 Concheiro, C. Alvarez-lorenzo, Polypseudorotaxanes of Pluronic ® F127 with  
905 Combinations of  $\alpha$  - and  $\beta$  -Cyclodextrins for Topical Formulation of Acyclovir,  
906 *Nanomaterials.* (2020). <https://doi.org/10.3390/nano10040613>.
- 907 [15] L.C. Gonçalves, A.B. Seabra, M.T. Pelegriño, D.R. De Araujo, J.S. Bernardes,  
908 Superparamagnetic iron oxide nanoparticles dispersed in Pluronic F127 hydrogel :  
909 potential uses in topical applications, *RSC Adv.* (2017) 14496–14503.  
910 <https://doi.org/10.1039/C6RA28633J>.
- 911 [16] M. Valero, C.A. Dreiss, Modulating Pluronics micellar rupture with cyclodextrins  
912 and drugs: Effect of pH and temperature, in: *J. Phys. Conf. Ser.*, 2014.  
913 <https://doi.org/10.1088/1742-6596/549/1/012010>.
- 914 [17] M. Valero, C.A. Dreiss, Growth, shrinking, and breaking of pluronic micelles in  
915 the presence of drugs and/or  $\beta$ -cyclodextrin, a study by small-angle neutron  
916 scattering and fluorescence spectroscopy, *Langmuir.* 26 (2010).  
917 <https://doi.org/10.1021/la100596q>.
- 918 [18] M. Valero, F. Castiglione, A. Mele, M.A. Da Silva, I. Grillo, G. González-  
919 Gaitano, C.A. Dreiss, Competitive and Synergistic Interactions between Polymer  
920 Micelles, Drugs, and Cyclodextrins: The Importance of Drug Solubilization  
921 Locus, *Langmuir.* 32 (2016). <https://doi.org/10.1021/acs.langmuir.6b03367>.
- 922 [19] G. Wenz, B.H. Han, A. Müller, Cyclodextrin rotaxanes and polyrotaxanes, *Chem.*  
923 *Rev.* 106 (2006) 782–817. <https://doi.org/10.1021/cr970027+>.
- 924 [20] K. Kataoka, A. Harada, Y. Nagasaki, Block copolymer micelles for drug delivery:

- 925 design, characterization and biological significance, *Adv. Drug Deliv. Rev.* 47  
 926 (2001) 113–131. [https://doi.org/10.1016/s0169-409x\(00\)00124-1](https://doi.org/10.1016/s0169-409x(00)00124-1).
- 927 [21] G. González-Gaitano, C. Müller, A. Radulescu, C.A. Dreiss, Modulating the self-  
 928 assembly of amphiphilic X-shaped block copolymers with cyclodextrins:  
 929 Structure and mechanisms, *Langmuir*. 31 (2015) 4096–4105.  
 930 <https://doi.org/10.1021/acs.langmuir.5b00334>.
- 931 [22] J. Puig-Rigall, I. Grillo, C.A. Dreiss, G. González-Gaitano, Structural and  
 932 Spectroscopic Characterization of TPGS Micelles: Disruptive Role of  
 933 Cyclodextrins and Kinetic Pathways, *Langmuir*. 33 (2017) 4737–4747.  
 934 <https://doi.org/10.1021/acs.langmuir.7b00701>.
- 935 [23] J. Puig-Rigall, R. Serra-Gómez, N. Guembe-Michel, I. Grillo, C.A. Dreiss, G.  
 936 González-Gaitano, Threading Different Rings on X-Shaped Block Copolymers:  
 937 Hybrid Pseudopolyrotaxanes of Cyclodextrins and Tetronics, *Macromolecules*.  
 938 (2020). <https://doi.org/10.1021/acs.macromol.0c00409>.
- 939 [24] M. Valero, I. Grillo, C.A. Dreiss, Rupture of pluronic micelles by Di-methylated  
 940  $\beta$ -cyclodextrin is not due to polypseudorotaxane formation, *J. Phys. Chem. B*. 116  
 941 (2012). <https://doi.org/10.1021/jp210439n>.
- 942 [25] E.N. Loredana, A.P. Chiriac, M. Bercea, Effect of pH and temperature upon self-  
 943 assembling process between poly(aspartic acid) and Pluronic F127, *Colloids  
 944 Surfaces B Biointerfaces*. 119 (2014) 47–54.  
 945 <https://doi.org/10.1016/j.colsurfb.2014.04.023>.
- 946 [26] S. Alexander, W.M. De Vos, T.C. Castle, T. Cosgrove, S.W. Prescott, Growth  
 947 and shrinkage of pluronic micelles by uptake and release of flurbiprofen:  
 948 Variation of pH, *Langmuir*. 28 (2012) 6539–6545.  
 949 <https://doi.org/10.1021/la204262w>.
- 950 [27] P. Parekh, R. Ganguly, V.K. Aswal, P. Bahadur, Room temperature sphere-to-rod  
 951 growth of Pluronic® P85 micelles induced by salicylic acid, *Soft Matter*. 8 (2012)  
 952 5864–5872. <https://doi.org/10.1039/c2sm25517k>.
- 953 [28] M. Khimani, G. Verma, S. Kumar, P.A. Hassan, V.K. Aswal, P. Bahadur, pH  
 954 induced tuning of size, charge and viscoelastic behavior of aqueous micellar  
 955 solution of Pluronic®P104–anthranilic acid mixtures: A scattering, rheology and  
 956 NMR study, *Colloids Surfaces A Physicochem. Eng. Asp.* 470 (2015) 202–210.  
 957 <https://doi.org/10.1016/j.colsurfa.2015.01.051>.
- 958 [29] Y. Kadam, U. Yerramilli, A. Bahadur, P. Bahadur, Micelles from PEO-PPO-PEO  
 959 block copolymers as nanocontainers for solubilization of a poorly water soluble  
 960 drug hydrochlorothiazide, *Colloids Surf. BBiointerface*. 83 (2011) 49–57.  
 961 <https://doi.org/10.1016/j.colsurfb.2010.10.041>.
- 962 [30] M.R. Montinari, S. Minelli, R. De Caterina, The first 3500 years of aspirin history  
 963 from its roots – A concise summary, *Vascul. Pharmacol.* 113 (2019) 1–8.  
 964 <https://doi.org/10.1016/j.vph.2018.10.008>.
- 965 [31] C.C. d. Lima Silva, H.M. Shimo, R. de Felício, G.F. Mercaldi, S.A. Rocco, C.E.  
 966 Benedetti, Structure–function relationship of a citrus salicylate methylesterase and  
 967 role of salicylic acid in citrus canker resistance, *Sci Rep* 9. 3901 (2019) 3901.  
 968 <https://doi.org/10.1038/s41598-019-40552-3>.
- 969 [32] S.J. Bashir, F. Dreher, A.L. Chew, H. Zhai, C. Levin, R. Stern, H.I. Maibach,  
 970 Cutaneous bioassay of salicylic acid as a keratolytic, *Int. J. Pharm.* 92 (2005)  
 971 187–194. <https://doi.org/doi:10.1016/j.ijpharm.2004.11.032>.
- 972 [33] F. Food and Drug Administration, Title 21, volume 5, n.d.
- 973 [34] R. Labib, D. Bury, F. Boisleve, G. Eichenbaum, S. Girard, J. Naciff, M. Leal, J.  
 974 Wong, A kinetic-based safety assessment of consumer exposure to salicylic acid

- 975 from cosmetic products demonstrates no evidence of a health risk from  
976 developmental toxicity, *Regul. Toxicol. Pharmacol.* 94 (2018) 245–251.  
977 <https://doi.org/10.1016/j.yrtph.2018.01.026>.
- 978 [35] M. Almgren, F. Grieser, J.K. Thomas, Dynamic and static aspects of  
979 solubilization of neutral arenes in ionic micellar solutions, *J. Am. Chem. Soc.* 101  
980 (1997) 279–291. <https://doi.org/10.1021/ja00496a001>.
- 981 [36] G. Song, R. Guo, Y. Y.F, Fluorimetric determination of binding constants and  
982 distribution coefficients of ethanol in the SDS micelles system, *Yangzhou*  
983 *Technol.Coll. (Nat.Sci.)*. 12 (1992) 42–47.
- 984 [37] A. Radulescu, N.K. Szekely, M.S. Appavou, V. Pipich, T. Kohnke, V. Ossovyi, S.  
985 Staringer, G.J. Schneider, M. Amann, B. Zhang-Haagen, G. Brandl, M. Drochner,  
986 R. Engels, R. Hanslik, G. Kemmerling, Studying soft-matter and biological  
987 systems over a wide length-scale from nanometer and micrometer sizes at the  
988 small-angle neutron diffractometer KWS-2, *J. Vis. Exp.* 2016 (2016) 1–23.  
989 <https://doi.org/10.3791/54639>.
- 990 [38] M. Doucet, J.H. Cho, G. Alina, J. Bakker, W. Bouwman, P. Butler, K. Campbell,  
991 M. Gonzales, R. Heenan, A. Jackson, P. Juhas, S. King, P. Kienzle, J. Krzywon,  
992 A. Markvardsen, T. Nielsen, L. O’Driscoll, W. Potrzebowski, R. Ferraz Leal, T.  
993 Richter, P. Rozycko, T. Snow, A. Washington, SasView version 4.2.2, (2019).  
994 <https://doi.org/10.5281/ZENODO.2652478>.
- 995 [39] A. and G.F. Guinier, *Small-Angle Scattering of X-Ray*, John Wiley & Sons Inc,  
996 new York, 1955.
- 997 [40] I. Livsey, *Neutron Scattering from Concentric Cylinders*, *J. Chem. Soc., Faraday*  
998 *Trans. 2.* 83 (1987) 1445–1452.
- 999 [41] S.R. Kline, Reduction and analysis of SANS and USANS data using IGOR Pro, *J.*  
1000 *Appl. Crystallogr.* 39 (2006) 895–900.  
1001 <https://doi.org/10.1107/S0021889806035059>.
- 1002 [42] I. Grillo, I. Morfin, S. Prévost, Structural Characterization of Pluronic Micelles  
1003 Swollen with Perfume Molecules, *Langmuir.* 34 (2018) 13395–13408.  
1004 <https://doi.org/10.1021/acs.langmuir.8b03050>.
- 1005 [43] O. Glatter, O. Kratky, eds., *Small Angle X-ray Scattering*, Academic Press, 1982.
- 1006 [44] J.S. Higgins, H.C. Benoit, *Polymers and Neutron Scattering*, Oxford Science  
1007 Publications, 1996.
- 1008 [45] S.M. King, *Small Angle Neutron Scattering in Modern Techniques for Polymer*  
1009 *Characterisation*, Wiley, 1999.
- 1010 [46] G. González-Gaitano, M.A. Da Silva, A. Radulescu, C.A. Dreiss, Selective tuning  
1011 of the self-assembly and gelation of a hydrophilic poloxamine by cyclodextrins,  
1012 *Langmuir.* 31 (2015) 5645–5655. <https://doi.org/10.1021/acs.langmuir.5b01081>.
- 1013 [47] R. Serra-Gómez, C.A. Dreiss, J. González-Benito, G. González-Gaitano,  
1014 Structure and rheology of poloxamine T1107 and its nanocomposite hydrogels  
1015 with cyclodextrin-modified barium titanate nanoparticles, *Langmuir.* 32 (2016)  
1016 6398–6408. <https://doi.org/10.1021/acs.langmuir.6b01544>.
- 1017 [48] J.H. Collett, R. Withington, Partition coefficients of salicylic acid between water  
1018 and the micelles of some non-ionic surfactants, *J. Pharm. Pharmacol.* 24 (1972)  
1019 211–214. <https://doi.org/10.1111/j.2042-7158.1972.tb08966.x>.
- 1020 [49] DrugBank, Salicylic acid, (2020).
- 1021 [50] Computed Properties by XLogP3 3.0 (PubChem release 2019.06.18), (n.d.).  
1022 <https://pubchem.ncbi.nlm.nih.gov/compound/156391> (accessed September 8,  
1023 2020).
- 1024 [51] <https://pubchem.ncbi.nlm.nih.gov/compound/Naproxen>(accessed May 20, 2020),,

- 1025 (n.d.).
- 1026 [52] A. Choucair, A. Eisenberg, Interfacial Solubilization of Model Amphiphilic  
1027 Molecules in Block Copolymer Micelles, *J. Am. Chem. Soc.* 125 (2003) 11993–  
1028 12000. <https://doi.org/10.1021/ja036667d>.
- 1029 [53] F. Gadelle, W.J. Koros, R.S. Schechter, Solubilization of Aromatic Solutes in  
1030 Block Copolymers, *Macromolecules*. 28 (1995) 4883–4892.  
1031 <https://doi.org/10.1021/ma00118a014>.
- 1032 [54] H.C. Joshi, H.B. Tripathi, T.C. Pant, D.D. Pant, Hydrogen-bonding effect on the  
1033 dual emission of salicylic acid, *Chem. Phys. Lett.* 173 (1990) 83–86.  
1034 [https://doi.org/10.1016/0009-2614\(90\)85307-X](https://doi.org/10.1016/0009-2614(90)85307-X).
- 1035 [55] H.C. Joshi, H. Mishra, H.B. Tripathi, Photophysics and photochemistry of  
1036 salicylic acid revisited, *J. Photochem. Photobiol. A Chem.* 105 (1997) 15–20.  
1037 [https://doi.org/10.1016/S1010-6030\(96\)04565-0](https://doi.org/10.1016/S1010-6030(96)04565-0).
- 1038 [56] D.D. Pant, H.C. Joshi, P.B. Bisht, H.B. Tripathi, Dual emission and double proton  
1039 transfer in salicylic acid, *Chem. Phys.* 185 (1994) 137–144.  
1040 [https://doi.org/10.1016/0301-0104\(94\)00090-5](https://doi.org/10.1016/0301-0104(94)00090-5).
- 1041 [57] S. Maheshwari, A. Chowdhury, N. Sathyamurthy, H. Mishra, H.B. Tripathi, M.  
1042 Panda, J. Chandrasekhar, Ground and Excited State Intramolecular Proton  
1043 Transfer in Salicylic Acid: An Ab Initio Electronic Structure Investigation, *J.*  
1044 *Phys. Chem. A*. 103 (1999) 6257–6262. <https://doi.org/10.1021/jp9911999>.
- 1045 [58] H.C. Joshi, C. Gooijer, G. Van der Zwan, Water-induced quenching of salicylic  
1046 anion fluorescence, *J. Phys. Chem. A*. 106 (2002) 11422–11430.  
1047 <https://doi.org/10.1021/jp020442s>.
- 1048 [59] R.N. de Souza, M.Z. Jora, L.G.T.A. Duarte, K.J. Clinckspoor, T.D.Z. Atvars, E.  
1049 Sabadini, A new interpretation of the mechanism of wormlike micelle formation  
1050 involving a cationic surfactant and salicylate, *J. Colloid Interface Sci.* 552 (2019)  
1051 794–800. <https://doi.org/10.1016/j.jcis.2019.05.025>.
- 1052 [60] H. Mishra, V. Misra, M.S. Mehata, T.C. Pant, H.B. Tripathi, Fluorescence Studies  
1053 of Salicylic Acid Doped Poly(vinyl alcohol) Film as a Water/Humidity Sensor, *J.*  
1054 *Phys. Chem. A*. 108 (2004) 2346–2352. <https://doi.org/10.1021/jp0309365>.
- 1055 [61] R.K. Rodrigues, M.A. Da Silva, E. Sabadini, Worm-like micelles of CTAB and  
1056 sodium salicylate under turbulent flow, *Langmuir*. 24 (2008) 13875–13879.  
1057 <https://doi.org/10.1021/la802890x>.
- 1058 [62] J. V. Joshi, V.K. Aswal, P.S. Goyal, Effect of sodium salicylate on the structure  
1059 of micelles of different hydrocarbon chain lengths, *Phys. B Condens. Matter*. 391  
1060 (2007) 65–71. <https://doi.org/10.1016/j.physb.2006.08.050>.
- 1061 [63] P.B. Bisht, H. Petek, K. Yoshihara, U. Nagashima, Excited state enol-keto  
1062 tautomerization in salicylic acid: A supersonic free jet study, *J. Chem. Phys.* 103  
1063 (1995) 5290–5307. <https://doi.org/10.1063/1.470565>.
- 1064 [64] G.S. Denisov, N.S. Golubev, V.M. Schreiber, S.S. Shajakhmedov, A. V.  
1065 Shurukhina, Effect of intermolecular hydrogen bonding and proton transfer on  
1066 fluorescence of salicylic acid, *J. Mol. Struct.* 436–437 (1997) 153–160.  
1067 [https://doi.org/10.1016/S0022-2860\(97\)00136-1](https://doi.org/10.1016/S0022-2860(97)00136-1).
- 1068 [65] S. Imadul Islam, A. Das, R.K. Mitra, Excited state proton transfer in reverse  
1069 micelles: Effect of temperature and a possible interplay with solvation, *J.*  
1070 *Photochem. Photobiol. A Chem.* 404 (2021).  
1071 <https://doi.org/10.1016/j.jphotochem.2020.112928>.
- 1072 [66] D.L. Sackett, J. Wolff, Nile red as a polarity-sensitive fluorescent probe of  
1073 hydrophobic protein surfaces, *Anal. Biochem.* 167 (1987) 228–234.  
1074 [https://doi.org/10.1016/0003-2697\(87\)90157-6](https://doi.org/10.1016/0003-2697(87)90157-6).

- 1075 [67] D.L. Sackett, J.R. Knutson, J. Wolff, Hydrophobic surfaces of tubulin probed by  
1076 time-resolved and steady-state fluorescence of Nile Red, *J. Biol. Chem.* 265  
1077 (1990) 14899–14906.
- 1078 [68] A.M. Klinkner, P.J. Bugelski, C.R. Waites, C. Louden, T.K. Hart, W.D. Kerns, A  
1079 novel technique for mapping the lipid composition of atherosclerotic fatty streaks  
1080 by en face fluorescence microscopy, *J. Histochem. Cytochem.* 45 (1997) 743–  
1081 753. <https://doi.org/10.1177/002215549704500513>.
- 1082 [69] P. Greenspan, S.D. Fowler, Spectrofluorometric studies of the lipid probe, Nile  
1083 red, *J. Lipid Res.* 26 (1985) 781–789.
- 1084 [70] T.M.R. Viseu, G. Hungerford, A.F. Coelho, M.I.C. Ferreira, Dye-host interactions  
1085 for local effects recognition in homogeneous and nanostructured media, *J. Phys.*  
1086 *Chem. B.* 107 (2003) 13300–13312. <https://doi.org/10.1021/jp030284k>.
- 1087 [71] H. Tajalli, A.G. Gilani, M.S. Zakerhamidi, P. Tajalli, The photophysical  
1088 properties of Nile red and Nile blue in ordered anisotropic media, *Dye. Pigment.*  
1089 78 (2008) 15–24. <https://doi.org/10.1016/j.dyepig.2007.10.002>.
- 1090 [72] F. Palomba, D. Genovese, L. Petrizza, E. Rampazzo, N. Zaccheroni, L. Prodi,  
1091 Mapping heterogeneous polarity in multicompartiment nanoparticles, *Sci. Rep.* 8  
1092 (2018) 1–8. <https://doi.org/10.1038/s41598-018-35257-y>.
- 1093 [73] C.P. Smyth, *Dielectric Behavior and Structure*, McGraw Hill, 1955.
- 1094 [74] P. Walden, No Title, *Z. Phys.* 70 (1910) 569.
- 1095 [75] I. Grillo, I. Morfin, J. Combet, Chain conformation: A key parameter driving  
1096 clustering or dispersion in polyelectrolyte – Colloid systems, *J. Colloid Interface*  
1097 *Sci.* 561 (2020) 426–438. <https://doi.org/10.1016/j.jcis.2019.11.010>.
- 1098 [76] J.S. Pedersen, M.C. Gerstenberg, The structure of P85 Pluronic block copolymer  
1099 micelles determined by small-angle neutron scattering, *Colloids Surfaces A*  
1100 *Physicochem. Eng. Asp.* 213 (2003) 175–187. [https://doi.org/10.1016/S0927-7757\(02\)00511-3](https://doi.org/10.1016/S0927-7757(02)00511-3).
- 1102 [77] S. Manet, A. Lecchi, M. Impérator-Clerc, V. Zholobenko, D. Durand, C.L.P.  
1103 Oliveira, J.S. Pedersen, I. Grillo, F. Meneau, C. Rochas, Structure of micelles of a  
1104 nonionic block copolymer determined by SANS and SAXS, *J. Phys. Chem. B.*  
1105 115 (2011) 11318–11329. <https://doi.org/10.1021/jp200212g>.
- 1106 [78] H.H. Kim, N.W. Song, T.S. Park, M. Yoon, Laser scanning confocal microscope  
1107 (LSCM)-fluorescence spectral properties of Nile Red embedded in polystyrene  
1108 film of different thickness, *Chem. Phys. Lett.* 432 (2006) 200–204.  
1109 <https://doi.org/10.1016/j.cplett.2006.10.049>.
- 1110 [79] T.H. Kim, Y.S. Han, J.D. Jang, B.S. Seong, SANS study on self-assembled  
1111 structures of Pluronic F127 triblock copolymer induced by additives and  
1112 temperature, *J. Appl. Crystallogr.* 47 (2014) 53–59.  
1113 <https://doi.org/10.1107/S1600576713030094>.
- 1114 [80] K. Dehvari, K.-S. Lin, S.S.-S. Wang, Small angle x-ray scattering characterization  
1115 of multifunctional iron oxide-pluronic nanocarriers: Effect of temperature and  
1116 drug encapsulation, *Nanosci. Nanotechnol. Lett.* 8 (2016) 667–670.  
1117 <https://doi.org/doi:10.1166/nnl.2016.2210>.
- 1118 [81] J. Dey, S. Kumar, S. Nath, R. Ganguly, V.K. Aswal, K. Ismail, Additive induced  
1119 core and corona specific dehydration and ensuing growth and interaction of  
1120 Pluronic F127 micelles, *J. Colloid Interface Sci.* 415 (2014) 95–102.  
1121 <https://doi.org/10.1016/j.jcis.2013.10.019>.
- 1122 [82] V. Shah, B. Bharatiya, V. Patel, M.K. Mishra, A.D. Shukla, D.O. Shah,  
1123 Interaction of salicylic acid analogues with Pluronic® micelles: Investigations on  
1124 micellar growth and morphological transition, *J. Mol. Liq.* 277 (2019) 563–570.

- 1125 <https://doi.org/10.1016/j.molliq.2018.12.142>.
- 1126 [83] K. Kaizu, P. Alexandridis, Glucose-induced sphere to ellipsoid transition of  
1127 polyoxyethylene-polyoxypropylene block copolymer micelles in aqueous  
1128 solutions, *Colloids Surfaces A Physicochem. Eng. Asp.* 480 (2015) 203–213.  
1129 <https://doi.org/10.1016/j.colsurfa.2014.10.061>.
- 1130 [84] Y. Kadam, R. Ganguly, M. Kumbhakar, V.K. Aswal, P.A. Hassan, P. Bahadur,  
1131 Time Dependent Sphere-to-Rod Growth of the Pluronic Micelles: Investigating  
1132 the Role of Core and Corona Solvation in Determining the Micellar Growth Rate,  
1133 *J.Phys.Chem. B.* 113 (2009) 16296–16302. <https://doi.org/10.1021/jp9036974>.
- 1134 [85] J. Puig-Rigall, M.J. Blanco-Prieto, A. Radulescu, C.A. Dreiss, G. González-  
1135 Gaitano, Morphology, gelation and cytotoxicity evaluation of D- $\alpha$ -Tocopheryl  
1136 polyethylene glycol succinate (TPGS) – Tetronic mixed micelles, *J. Colloid  
1137 Interface Sci.* 582 (2021) 353–363. <https://doi.org/10.1016/j.jcis.2020.08.004>.
- 1138 [86] R. Basak, R. Bandyopadhyay, Encapsulation of hydrophobic drugs in pluronic  
1139 F127 micelles: Effects of drug hydrophobicity, solution temperature, and pH,  
1140 *Langmuir.* 29 (2013) 4350–4356. <https://doi.org/10.1021/la304836e>.
- 1141 [87] K.C. Shih, Z. Shen, Y. Li, M. Kröger, S.Y. Chang, Y. Liu, M.P. Nieh, H.M. Lai,  
1142 What causes the anomalous aggregation in pluronic aqueous solutions?, *Soft  
1143 Matter.* 14 (2018) 7653–7663. <https://doi.org/10.1039/c8sm01096j>.
- 1144 [88] Y. Wang, S.A. Sukhishvili, Hydrogen-bonded polymer complexes and nanocages  
1145 of weak polyacids templated by a Pluronic® block copolymer, *Soft Matter.* 12  
1146 (2016) 8744–8754. <https://doi.org/10.1039/c6sm01869f>.
- 1147 [89] S. Alexander, T. Cosgrove, T.C. Castle, I. Grillo, S.W. Prescott, Effect of  
1148 temperature, cosolvent, and added drug on pluronic-flurbiprofen micellization, *J.  
1149 Phys. Chem. B.* 116 (2012) 11545–11551. <https://doi.org/10.1021/jp303185m>.
- 1150 [90] C.A. Dreiss, E. Nwabunwanne, R. Liu, N.J. Brooks, Assembling and de-  
1151 assembling micelles: Competitive interactions of cyclodextrins and drugs with  
1152 Pluronics, *Soft Matter.* 5 (2009) 1888–1896. <https://doi.org/10.1039/b812805g>.
- 1153 [91] C. Perry, P. Hébraud, V. Gernigon, C. Brochon, A. Lapp, P. Lindner, G. Schlatter,  
1154 Pluronic and  $\beta$ -cyclodextrin in water: from swollen micelles to self-assembled  
1155 crystalline platelets, *Soft Matter.* 7 (2011) 3502–3512.  
1156 <https://doi.org/10.1039/C0SM01092H>.
- 1157 [92] E. Junquera, L. Peña, E. Aicart, Binding of sodium salicylate by  $\beta$ -cyclodextrin or  
1158 2,6-di-o-methyl- $\beta$ - cyclodextrin in aqueous solution, *J. Pharm. Sci.* 87 (1998) 86–  
1159 90. <https://doi.org/10.1021/js970117u>.
- 1160 [93] M. Khimani, G. Verma, S. Kumar, P.A. Hassan, V.K. Aswal, P. Bahadur, pH  
1161 induced tuning of size, charge and viscoelastic behavior of aqueous micellar  
1162 solution of Pluronic®P104–anthranilic acid mixtures: A scattering, rheology and  
1163 NMR study, *Colloids Surfaces A Physicochem. Eng. Asp.* 470 (2015) 202–210.  
1164 <https://doi.org/10.1016/j.colsurfa.2015.01.051>.
- 1165 [94] F. Castiglione, M. Valero, C.A. Dreiss, A. Mele, Selective interaction of 2,6-Di-  
1166 O-methyl- $\beta$ -cyclodextrin and pluronic F127 micelles leading to micellar rupture:  
1167 A nuclear magnetic resonance study, *J. Phys. Chem. B.* 115 (2011).  
1168 <https://doi.org/10.1021/jp203753r>.
- 1169 [95] R.C. Da Silva, W.J. Loh, Effect of Additives on the Cloud Points of Aqueous  
1170 Solutions of Ethylene Oxide–Propylene Oxide–Ethylene Oxide Block  
1171 Copolymers, *Colloid Interface Sci.* 202 (1998) 385–390.  
1172 <https://doi.org/https://doi.org/10.1006/jcis.1998.5456>.
- 1173 [96] C.D. Grant, K.E. Steege, M.R. Bunagan, E.W. Castner Jr, Microviscosity in  
1174 Multiple Regions of Complex Aqueous Solutions of Poly(ethylene oxide) oxide)-

1175 poly(propylene oxide) oxide)-poly(ethylene oxide), J. Phys. Chem. B. 109 (2005)  
1176 22273–22284. <https://doi.org/10.1021/jp053929k>.  
1177 [97] H. Schott, E.A. Royce, Colloids and Surfaces, 19 (1986), Colloids Surf. 19 (1986)  
1178 399–418.  
1179 [98] A.M. Al-Ghamdi, H.A. Nasr-E1-Din, SURFACES, Colloids Surfaces A  
1180 Physicochem. Eng. Asp. 125 (1997) 5–18.  
1181  
1182  
1183